

THE RADIOSITY EQUATION ON CERTAIN
SPACES OF CONTINUOUS FUNCTIONS
AND ITS NUMERICAL SOLUTION

OLAF HANSEN

ABSTRACT. In this article we study the radiosity equation on a polyhedral surface S in \mathbf{R}^3 . We construct a special space of continuous functions on S where we can prove the existence of a unique solution of the radiosity equation. These results enable us to construct grids for the numerical approximation of the solution which guarantee convergence in the maximum norm for the collocation method. In a last section we present numerical results which confirm our theoretical prediction and these results also show that graded meshes will increase the order of convergence.

1. Introduction. The exchange of energy by radiation is an important physical mechanism for heat transfer, see [19, 22–24], and for the calculation of 3D pictures in computer science, see [7, 20, 25]. For the heat transfer the exchange of energy by radiation is only one transport mechanism, besides diffusion and convection. The relative importance of these mechanisms depends on material properties and the surface temperature.

In contrast to this the radiation is the only process to consider in the calculation of 3D scenes in computer graphics. Here the sources of radiation are prescribed by lamps, which are distributed on the surface. In general the emitted radiation at every point depends on the direction. But in this article we will consider only surfaces where the radiance, see [19] for a definition, fulfills the Lambertian cosine law, which means that the radiance is constant in all directions. So this emitted radiation at every point can be characterized by a scalar, which determines the density of the emitted energy, and this quantity is called radiosity. To be consistent, we also must assume that all radiation sources are diffusive emitters. The resulting model does not contain any specular

Key words and phrases. Radiosity equation, integral equation, regularity theory, collocation method, graded meshes.

1991 AMS *Mathematics Subject Classification.* 45P05, 65R20, 68U05.

Received by the editors on July 12, 2001, and in revised form on May 3, 2002.

Copyright ©2003 Rocky Mountain Mathematics Consortium

effects. This model results in the following integral equation of the second kind for the radiosity $u : S \rightarrow \mathbf{R}_0^+$:

(1.1)

$$u(x) = E(x) + \frac{\rho(x)}{\pi} \int_S V(x, y) \frac{[\vec{n}(x) \cdot (y-x)][\vec{n}(y) \cdot (x-y)]}{\|x-y\|^4} u(y) ds_y,$$

$$x \in S.$$

Here S is the surface, where we want to calculate the radiosity. The surface S needn't be closed. The above equation implies that the radiation at every point is given by the source term $E(x)$ and the reflected fraction $\rho(x) \in [0, 1)$ of the incoming radiation. So $1/\pi$ times the integral on the righthand side of (1.1) gives the incoming radiation, see [19]. The function $V : S \times S \rightarrow \{0, 1\}$ is the visibility function which is equal to one if two points can exchange energy and otherwise zero. If S is the interior of a convex room, the function V is equal to one, but in situations where there are shadows the function V attains both values. In this article we will assume that the surface is the union of a finite number of triangles. Therefore a normal vector $\vec{n}(x)$ is defined for almost all points $x \in S$, which ensures that the integral in (1.1) is well defined.

Although there is a huge literature on the radiosity equation in computer graphics, see the references in [7, 20–25], there are not so many mathematical investigations on the structure, for example regularity, of the solution \bar{u} of (1.1). Existence theory in the $L^p(S)$ spaces, $p \in [1, \infty]$, or in spaces of continuous functions, under certain assumptions on S and E , can be found in [1, 3, 4, 10, 16, 17]. In [17] the properties of \bar{u} along an edge were studied, if the function E is differentiable and in [3] one finds results for the regularity of \bar{u} near corners in the two-dimensional cases. In [11] an L^2 theory for the regularity of \bar{u} along an edge was developed.

The content of our paper is the following. In Section 2 we study (1.1) in the space of continuous functions. We show that neither the space of continuous functions on S , with respect to the Euclidean topology, nor the space of piecewise (with respect to the underlying triangulation) continuous functions is well suited for (1.1). We introduce a space of continuous functions $\mathcal{C}_R(S)$, where the continuity near the vertices is defined with respect to polar coordinates. If the emission function E belongs to $\mathcal{C}_R(S)$, there is a unique solution of (1.1) in the same space,

see Theorem 2.14. Examples show that there is no existence theorem in the usual space of piecewise continuous functions. The main ingredient for the proof of Theorem 2.14 is Theorem 2.13, where we prove that the reflection operator is a continuous operator in the space $C_R(S)$. This existence theorem is the foundation for the use of the collocation method for the approximate solution of (1.1). The only thing one has to keep in mind is that no collocation points in the corners are allowed.

Another consequence is that we must use special meshes for the numerical scheme in order to guarantee pointwise convergence towards the solution of (1.1). For this purpose we must use meshes, which resolve the angular variable near the vertices. The construction of these meshes is given in Section 3, and a collocation method is described in detail. Our trial functions are dense in the space $\mathcal{C}_R(S)$ and therefore our collocation method converges in the maximum norm. To prove this we also need the stability, but this was already investigated in an earlier article [12]. The same kind of meshes must be used for the Galerkin method if one is interested in pointwise convergence. This result is independent of the particular trial functions, i.e., piecewise constant functions, linear or higher order polynomials.

In the last section we present numerical calculations for a simple test surface. The results show that we have to use meshes which resolve the angular variable in order to guarantee convergence in $L^\infty(S)$. The singular behavior of the derivative of the solution \bar{u} of (1.1) near edges or corners is also exhibited in the numerical results. This behavior was studied in [17, 10, 11] and it indicates that the use of graded meshes will result in better convergence results.

2. The radiosity equation on the space of continuous functions. In the following we will assume that the surface S is given in the following form

$$(2.1) \quad S = \bigcup_{j=1}^n \Delta_j, \quad \Delta_j \subset \mathbf{R}^3, \quad \text{plane bounded triangles.}$$

By n_j we denote one of the normals of Δ_j ; this determines the side of Δ_j which is part of our surface S . The triangles are closed and, by $\dot{\Delta}_j$ we denote the relative interior. If we think of S as the boundary of a polyhedral domain in \mathbf{R}^3 , it is clear that the intersection of two

triangles is either empty, an edge, a vertex or the whole triangle (in the case that there is a slit in the polyhedral domain). Also in the general case (2.1) we would like to consider only these four cases. So we assume that the intersection of two triangles is never a line in the interior of a triangle. If $\hat{\Delta}_j \cap \hat{\Delta}_k \neq \emptyset$, $j \neq k$, then $n_j = -n_k$. We further denote by \mathcal{K}_S the integral operator on the righthand side of equation (1.1),

(2.2)

$$(\mathcal{K}_S u)(x) := \frac{\rho(x)}{\pi} \int_S V(x, y) \frac{[\vec{n}(x) \cdot (y-x)][\vec{n}(y) \cdot (x-y)]}{\|x-y\|^4} u(y) ds_y,$$

$$x \in S.$$

and this operator will be called *reflection operator*. Furthermore, we assume that the reflectivity is piecewise constant

$$(2.3) \quad \rho|_{\Delta_j} \equiv \rho_j \in [0, 1), \quad j = 1(1)n.$$

Because the surface S is the union of plane triangles we can equip S with the two-dimensional Lebesgue measure ds_y , as we have already done in the definition of the radiosity equation, and define the spaces $L^p(S)$, $p \in [1, \infty]$. In [1, 16] it was shown that

$$(2.4) \quad \|\mathcal{K}_S\|_{L^p(S) \rightarrow L^p(S)} \leq \rho_{\mathcal{K}_S} := \max_{j=1}^n \rho_j < 1$$

holds. This implies the unique solvability of the radiosity equation

$$(2.5) \quad (I - \mathcal{K}_S)u = E, \quad E \in L^p(S).$$

The solution $\bar{u} \in L^p(S)$ is given by the Neumann series

$$(2.6) \quad \bar{u} = \sum_{j=0}^{\infty} (\mathcal{K}_S)^j E.$$

The calculation of a finite part of the Neumann series in order to get an approximate solution is one of the methods which are used in practical calculations, see [13].

The above results are not enough to justify the use of the collocation method for the approximate solution of (2.5) because we need point evaluations (but compare [4] for the case of a smooth surface). Since

the reflection operator looks similar to the double layer operator, see [14], one might think that a solution theory in the space of continuous or piecewise continuous functions is possible. One of the results of this section is that this is not the case. We must use a larger space which we describe in the next definition.

Definition 2.1. By $\mathcal{C}_P(S)$ (here P means piecewise) we denote the set of functions on S given in the following way

$$\begin{aligned} u \in \mathcal{C}_P(S) &\implies u = (u_1, \dots, u_n), \\ u_j &: \Delta_j \rightarrow \mathbf{R}, \quad u_j \in \mathcal{C}(\dot{\Delta}_j), \end{aligned}$$

such that each u_j has a continuous extension to Δ_j . The norm on the Banach space $\mathcal{C}_P(S)$ is given by

$$(2.7) \quad \|u\|_{\mathcal{C}_P(S)} := \|u\|_{L^\infty(S)}.$$

The Banach space $\mathcal{C}(S) \subset \mathcal{C}_P(S)$ is defined by

$$u \in \mathcal{C}(S) \implies u \in \mathcal{C}_P(S),$$

if Δ_j and Δ_k have a common point x which belongs to an edge, then $u_j(x) = u_k(x)$.

The next Banach space $\mathcal{C}_R(S), \mathcal{C}_P(S) \subset \mathcal{C}_R(S)$ is defined by local polar coordinates around each corner.

$$\begin{aligned} u \in \mathcal{C}_R(S) &\implies u = (u_1, \dots, u_n), \\ u_j &: \Delta_j \rightarrow \mathbf{R}, \quad u_j \in \mathcal{C}(\dot{\Delta}_j), \end{aligned}$$

and if we assume that Δ_j has the vertices $v_1^{(j)}, v_2^{(j)}$ and $v_3^{(j)}$, then the following conditions must be satisfied. Let r and ϕ be the polar coordinates around vertex $v_i^{(j)}$, $i \in \{1, 2, 3\}$, $r \in [0, r_i]$, $r_i := \min_{k \neq i} \{\|v_k^{(j)} - v_i^{(j)}\|\}$, $\phi \in [\phi_1, \phi_2]$. Then $u_j = u_j(r, \phi)$ should be continuous on $B_i := ([0, r_i/2] \times [\phi_1, \phi_2]) \cap \Delta_j$. Furthermore, u_j should be continuous on the closure of $\Delta_j \setminus (B_1 \cup B_2 \cup B_3)$. The norm $\|\cdot\|_{\mathcal{C}_R(S)}$ is also given by

$$\|u\|_{\mathcal{C}_R(S)} := \|u\|_{L^\infty(S)}.$$

All three spaces carry the same norm, and we get

$$\mathcal{C}(S) \subset \mathcal{C}_P(S) \subset \mathcal{C}_R(S).$$

Remark 2.2. a. The definition of $\mathcal{C}(S)$ is made in such a way, that in the case $\Delta_j = \Delta_k$, $n_j = -n_k$, the functions u_j and u_k have no relation in the interior of their domain of definition, but along the common edges these two functions should coincide.

b. In this section we will see that the space $\mathcal{C}_R(S)$ is better suited for the study of the reflection operator \mathcal{K}_S than the spaces $\mathcal{C}_P(S)$ or $\mathcal{C}(S)$. But the functions in $\mathcal{C}_R(S)$ are in general not piecewise continuous with respect to the Euclidean geometry on S .

c. In Definition 2.1 it is assumed that all triangles Δ_j , $j = 1(1)n$, are bounded. But we will use the above defined spaces also in the case that some Δ_k are infinite plane sections in \mathbf{R}^3

$$\begin{aligned} \Delta_k = \{x + r(\cos(\alpha)e_1 + \sin(\alpha)e_2) \mid r \geq 0, \alpha \in [\alpha_1, \alpha_2]\}, \\ e_1, e_2 \in \mathbf{R}^3, \|e_1\| = \|e_2\| = 1, e_1 \cdot e_2 = 0, \\ x \in \mathbf{R}^3, \alpha_1 < \alpha_2. \end{aligned}$$

This does not cause any problems.

One of the major tools for the study of the double layer operator is the geometrical interpretation of $W_S \mathbf{1}(x)$, $x \notin S$. Here $\mathbf{1}$ denotes the function which is constant to 1 on S and W_S denotes the double layer operator on S . If S is for example one triangle, then $W_S \mathbf{1}(x)$ is just the normalized solid angle of S seen from x . This fact is one of the arguments used by Král to prove that W_S maps continuous functions on continuous functions, see [14].

A similar interpretation holds for $\mathcal{K}_S \mathbf{1}(x)$, which is called differential form factor. We present this in result Lemma 2.4. But first we define some geometric objects for the formulation of Lemma 2.4.

Definition 2.3. Given a point $x \in \mathbf{R}^3$ and a vector $n \in \mathbf{R}^3$, $\|n\| = 1$, let $S_{n,\varepsilon}^2(x)$ be the half sphere

$$(2.8) \quad S_{n,\varepsilon}^2(x) := \{y \in \mathbf{R}^3 \mid \|x - y\| = \varepsilon, n \cdot (y - x) \geq 0\}$$

with bottom surface

$$(2.9) \quad B_{n,\varepsilon}^2(x) := \{y \in \mathbf{R}^3 \mid \|x - y\| \leq \varepsilon, n \cdot (y - x) = 0\}.$$

For a set $A \subset \mathbf{R}^3$, $\text{dist}(x, A) > \varepsilon$, we define the projection

$$(2.10) \quad P(A) := \{y \in S_{n,\varepsilon}^2(x) \mid \exists \lambda \geq 1, x + \lambda(y - x) \in A\}$$

on $S_{n,\varepsilon}^2(x)$ and the projection of $P_\perp(A)$ on the bottom surface

$$(2.11) \quad P_\perp(A) := \{y - [n \cdot (y - x)]n \mid y \in P(A)\},$$

see the following figure.

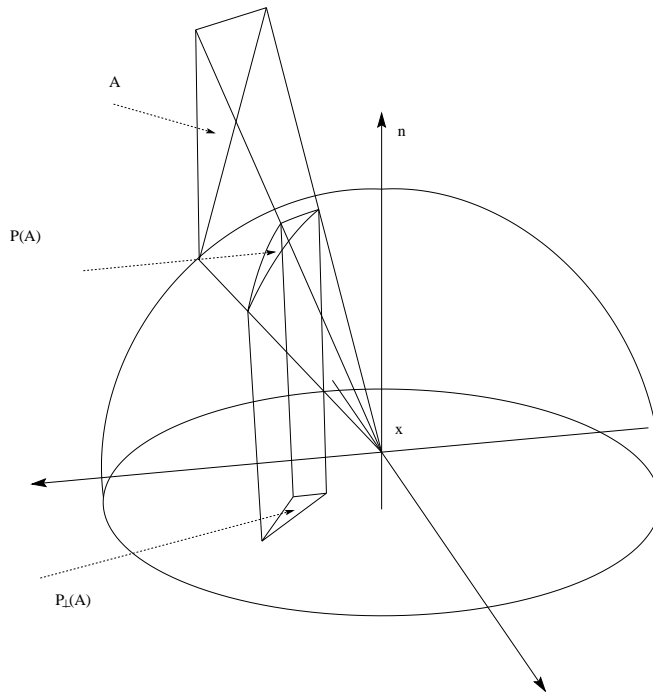


FIGURE 2.1. Definition of $P(A)$ and $P_\perp(A)$.

In both cases we have not indicated the dependence on x , n and ε , but one has to keep this in mind.

The choice of ε guarantees that the volume $V(A)$

$$(2.12) \quad V(A) := \left\{ x + r \frac{y-x}{\|y-x\|} \mid \varepsilon \leq r \leq \|y-x\|, y \in A \right\}$$

is enclosed on two sides by A and $P(A)$. If we denote by μ the Lebesgue surface measure on $S_{n,\varepsilon}^2(x)$, respectively $B_{n,\varepsilon}^2(x)$, and assume that the set A is not too irregular (it will always be a polygon in our applications), then it is clear that the real number

$$(2.13) \quad \frac{\mu(P_\perp(A))}{\mu(B_{n,\varepsilon}^2(x))} = \frac{\mu(P_\perp(A))}{\pi\varepsilon^2} =: \sigma_{x,n}(A)$$

exists and is independent of $\varepsilon \in (0, \text{dist}(A, x))$. It describes the relative area which is occupied by the normal projection of $P(A)$ onto $B_{n,\varepsilon}^2(x)$.

Given an orthonormal base e_1, e_2 and n of \mathbf{R}^3 we will denote by $E_{e_1, e_2, n}$ the plane

$$(2.14) \quad E_{e_1, e_2, n} := \{ \lambda e_1 + \mu e_2 \mid \lambda, \mu \in \mathbf{R} \}.$$

For any point $x \in E_{e_1, e_2, n}$ we can speak of a normal $n(x) = n$. The infinite sector $S_{e_1, e_2}(\alpha_1, \alpha_2) \subset E_{e_1, e_2, n}$, $0 \leq \alpha_1 < \alpha_2 \leq 2\pi$, is defined by

$$(2.15) \quad S_{e_1, e_2}(\alpha_1, \alpha_2) := \{ r(\cos(\alpha)e_1 + \sin(\alpha)e_2) \mid r \geq 0, \alpha \in [\alpha_1, \alpha_2] \}.$$

This means that, for $x \in S_{e_1, e_2}(\alpha_1, \alpha_2)$, there is always a well-defined normal $n(x) = n$.

For a set S , either a finite union of triangles or infinite sectors with given normal, we define a special reflection operator with reflectivity function $\rho \equiv 1$ and no visibility function V ,

$$(2.16) \quad (\overline{\mathcal{K}}_S u(x)) := \frac{1}{\pi} \int_S \frac{[n(x) \cdot (y-x)][n(y) \cdot (x-y)]}{\|x-y\|^4} u(y) ds_y.$$

The next lemma presents a geometrical interpretation for the differential form factor which can be found for example in the book of Moon

[15]. Moon calls this the solid-angle method. We are not interested in the explicit calculations of form factors here, but the result is useful to study continuity properties of $\mathcal{K}_S u$, u continuous. Therefore we present it here for the special case of two sectors.

Lemma 2.4. *Given two sets $\{e_1^{(1)}, e_2^{(1)}, n^{(1)}\}$ and $\{e_1^{(2)}, e_2^{(2)}, n^{(2)}\}$ of orthonormal bases of \mathbf{R}^3 we consider the two sectors*

$$\begin{aligned} S^{(1)} &:= S_{e_1^{(1)}, e_2^{(1)}}(\alpha_1, \alpha_2) \subset E_{e_1^{(1)}, e_2^{(1)}, n^{(1)}}, \quad \alpha_1 < \alpha_2, \\ S^{(2)} &:= S_{e_1^{(2)}, e_2^{(2)}}(\beta_1, \beta_2) \subset E_{e_1^{(2)}, e_2^{(2)}, n^{(2)}}, \quad \beta_1 < \beta_2, \end{aligned}$$

such that $S^{(1)} \cap S^{(2)}$ is either $\{0\}$ or an edge. Further we assume that all points of $S^{(1)}$ and $S^{(2)}$ can ‘see’ each other. If we parametrize the points $x \in S^{(2)}$ by

$$(2.17) \quad x = x(r, \beta) := r(\cos(\beta)e_1^{(2)} + \sin(\beta)e_2^{(2)}), \quad \beta \in [\beta_1, \beta_2],$$

we get

$$(\overline{\mathcal{K}}_S \mathbf{1})(x(r, \beta)) = (\overline{\mathcal{K}}_{S^{(1)}} \mathbf{1})(x(1, \beta)) = \sigma_{x(1, \beta), n^{(2)}}(S^{(1)}).$$

Proof. We introduce a similar parametrization to (2.17) for $S^{(1)}$.

$$y = y(r', \alpha) := r'(\cos(\alpha)e_1^{(1)} + \sin(\alpha)e_2^{(1)}), \quad r' \geq 0, \quad \alpha \in [\alpha_1, \alpha_2].$$

First we show that

$$(\overline{\mathcal{K}}_{S^{(1)}} \mathbf{1})(x(r, \beta))$$

is independent of r . This follows by the homogeneity of the kernel, but we give a formal proof.

$$\begin{aligned} (\overline{\mathcal{K}}_{S^{(1)}} \mathbf{1})(x(r, \beta)) &= \frac{1}{\pi} \int_{S^{(1)}} \frac{[n^{(2)} \cdot (y - x(r, \beta))][n^{(1)} \cdot (x(r, \beta) - y)]}{\|y - x(r, \beta)\|^4} ds_y \\ &= \frac{1}{\pi} \int_{S^{(1)}} \frac{[n^{(2)} \cdot y(r', \alpha)][n^{(1)} \cdot x(r, \beta)]}{\|y(r', \alpha) - x(r, \beta)\|^4} r' dr' d\alpha \\ &= \frac{1}{\pi} \int_{S^{(1)}} \frac{r(r')^2 a(\alpha) b(\beta)}{(r^2 - 2rr'c(\alpha, \beta) + (r')^2)^2} dr' d\alpha. \end{aligned}$$

Here we have defined

$$(2.18) \quad a(\alpha) := \cos(\alpha)n^{(2)} \cdot e_1^{(1)} + \sin(\alpha)n^{(2)} \cdot e_2^{(1)} \geq 0,$$

$$(2.19) \quad b(\beta) := \cos(\beta)n^{(1)} \cdot e_1^{(2)} + \sin(\beta)n^{(1)} \cdot e_2^{(2)} \geq 0,$$

$$(2.20)$$

$$c(\alpha, \beta) := (\cos(\alpha)e_1^{(1)} + \sin(\alpha)e_2^{(1)})(\cos(\beta)e_1^{(2)} + \sin(\beta)e_2^{(2)}) \in [-1, 1],$$

and this notation will be used frequently in the following. Now we get

$$\begin{aligned} (\overline{\mathcal{K}}_{S^{(1)}} \mathbf{1})(x(r, \beta)) &= \frac{1}{\pi} \int_{\alpha_1}^{\alpha_2} \frac{1}{r} \int_0^\infty \frac{(r'/r)^2 a(\alpha) b(\beta)}{((r'/r)^2 - 2(r'/r)c(\alpha, \beta) + 1)^2} dr' d\alpha \\ &= \frac{1}{\pi} \int_{\alpha_1}^{\alpha_2} \int_0^\infty \frac{\nu^2 a(\alpha) b(\beta)}{(\nu^2 - 2\nu c(\alpha, \beta) + 1)^2} d\nu d\alpha \end{aligned}$$

which is independent of r . So we only have to calculate $(\overline{\mathcal{K}}_{S^{(1)}} \mathbf{1})(x(1, \beta))$, $\beta \in [\beta_1, \beta_2]$. Let $\beta \in (\beta_1, \beta_2)$ and choose $\varepsilon > 0$ small enough to guarantee

$$S_{n^{(2)}, \varepsilon}^2(x(1, \beta)) \cap S^{(1)} = \emptyset.$$

By an easy calculation we get

$$\operatorname{div}_y \left(\frac{[n^{(2)} \cdot (y - x(1, \beta))](x(1, \beta) - y)}{\|x(1, \beta) - y\|^4} \right) = 0,$$

$y \in \mathbf{R}^3 \setminus \{x(1, \beta)\}$. The divergence theorem of Gauß applied to the volume $V(S^{(1)})$ between $S^{(1)}$ and $P(S^{(1)})$, see Definition 2.3, shows

$$\begin{aligned} (\overline{\mathcal{K}}_{S^{(1)}} \mathbf{1})(x(1, \beta)) &= \frac{1}{\pi} \int_{P(S^{(1)})} \frac{[n^{(2)} \cdot (y - x(1, \beta))]\|x(1, \beta) - y\|}{\|x(1, \beta) - y\|^4} ds_y \\ &= \frac{1}{\pi \varepsilon^3} \int_{P(S^{(1)})} n^{(2)} \cdot (y - x(1, \beta)) ds_y \\ &= \frac{1}{\pi \varepsilon^2} \int_{P_\perp(S^{(1)})} 1 ds_y \\ &= \sigma_{x(1, \beta), n^{(2)}}(S^{(1)}). \end{aligned}$$

This follows again by an easy calculation. \square

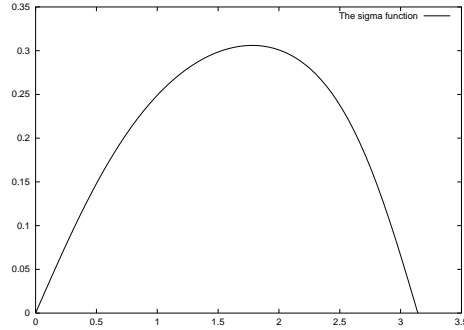


FIGURE 2.2. The function $\sigma_{x(1,\beta),n(2)}(S^{(1)})$, $\beta \in [0, \pi]$.

Remark 2.5. a. To get an impression of this function we draw $\sigma_{x(1,\beta),n(2)}(S^{(1)})$, $\beta \in [0, \pi]$ in Figure 2.2, if the following data are given

$$\begin{aligned}
 e_1^{(1)} &= \begin{pmatrix} 1 \\ 0 \\ 0 \end{pmatrix}, & e_2^{(1)} &= \begin{pmatrix} 0 \\ 1 \\ 0 \end{pmatrix}, \\
 n^{(1)} &= \begin{pmatrix} 0 \\ 0 \\ 1 \end{pmatrix}, & \alpha_1 &= \pi/3, \quad \alpha_2 = 3\pi/4, \\
 e_1^{(2)} &= \begin{pmatrix} 1 \\ 0 \\ 0 \end{pmatrix}, & e_2^{(2)} &= \begin{pmatrix} 0 \\ 0 \\ 1 \end{pmatrix}, \\
 n^{(2)} &= \begin{pmatrix} 0 \\ 1 \\ 0 \end{pmatrix}, & \beta_1 &= 0, \quad \beta_2 = \pi.
 \end{aligned}$$

b. Let $x \in \mathbf{R}^3$, $\|n\| = 1$ and $E \subset \mathbf{R}^3$ be a hyperplane such that

$$E \not\subset F := \{y \in \mathbf{R}^3 \mid (y - x) \cdot n = 0\}.$$

Further assume that $x \notin E$ and denote by n_E the normal of E such that $n_E \cdot (x - y) > 0$, $y \in E$. If

$$E_+ := \{y \in E \mid (y - x) \cdot n \geq 0\}$$

is the part of E which can be ‘seen’ from x , we get

$$(2.21) \quad \begin{aligned} \sigma_{x,n}(E_+) &= \frac{1}{\pi} \int_{E_+} \frac{[n \cdot (y-x)][n_E \cdot (x-y)]}{\|x-y\|^4} ds_y \\ &= \frac{1}{2}(1 + \cos(\gamma)) \end{aligned}$$

where γ is the angle between E and F on the side where the point x is located. This follows by a simple calculation from Lemma 2.4 and can be found for example in [15] or in Appendix A2 of [19].

c. If the two sectors $S^{(1)}$ and $S^{(2)}$ have a common edge, for example for $\alpha_1 = \beta_1 = 0$, the above comment shows

$$\begin{aligned} \lim_{\beta \searrow 0} (\overline{\mathcal{K}}_{S^{(1)}} \mathbf{1})(x(r, \beta)) &= \frac{1}{2}(1 + \cos(\gamma)) \\ &= \frac{1}{2}(1 + e_2^{(1)} \cdot e_2^{(2)}), \end{aligned}$$

where now γ is the angle between the planes generated by $S^{(1)}$ and $S^{(2)}$.

d. If $\alpha_1 = 0$, $\alpha_2 = \pi$, then $S^{(1)}$ is a half plane and all points of $S^{(2)}$ can see the whole of $S^{(1)}$. In this case we get

$$(\overline{\mathcal{K}}_{S^{(1)}} \mathbf{1})(x(1, \beta)) = \frac{1}{2}(1 + \cos(\gamma)), \quad \beta \in [\beta_1, \beta_2],$$

where γ is again the angle between $S^{(1)}$ and $S^{(2)}$. So $(\overline{\mathcal{K}}_{S^{(1)}} \mathbf{1})(x(r, \beta))$ is a constant function.

e. If $\alpha_1 > 0$ or $\alpha_2 < \pi$, then $S^{(1)}$ is not a half plane and

$$(\overline{\mathcal{K}}_{S^{(1)}} \mathbf{1})(x(1, \beta))$$

is not a constant function, $\beta \in [\beta_1, \beta_2]$. This implies that $(\overline{\mathcal{K}}_{S^{(1)}} \mathbf{1})(x(r, \beta))$ is not continuous on $S^{(2)}$, but

$$(\overline{\mathcal{K}}_{S^{(1)}} \mathbf{1})x(1, \beta) \in \mathcal{C}_R(S^{(2)}).$$

f. Lemma 2.4 is also true for more general objects than $S^{(1)}$. For example, for a triangle Δ we get

$$(\mathcal{K}_\Delta \mathbf{1})(x) = \sigma_{x,n^{(2)}}(\Delta),$$

if Δ can be seen from x .

A result of the above remark is

Corollary 2.6. *Given two sectors $S^{(1)}$ and $S^{(2)}$ according to Lemma 2.4, we have in general*

$$\overline{\mathcal{K}}_{S^{(1)}} : \mathcal{C}(S^{(1)}) \not\rightarrow \mathcal{C}(S^{(2)}).$$

Proof. Here it is enough to recall the example in Remark 2.5e,

$$(\overline{\mathcal{K}}_{S^{(1)}} \mathbf{1})(r, \phi) = \sigma_{x(1, \phi), n^{(2)}}(S^{(1)})$$

which is not a constant function with respect to ϕ . \square

Now we know that $\mathcal{K}_{S^{(1)}}$ does not map continuous functions onto continuous functions on $S^{(2)}$. But we know $\overline{\mathcal{K}}_S \mathbf{1} \in C_R(S^{(2)})$. So we hope that

$$(2.22) \quad \overline{\mathcal{K}}_{S^{(1)}} : C_R(S^{(1)}) \longmapsto C_R(S^{(2)})$$

is true. This will be shown in two steps. Lemma 2.7 proves $\overline{\mathcal{K}}_{S^{(1)}} u \in C_R(S^{(2)})$ for a function u which does not depend on the radial variable. Lemma 2.9 uses this result to prove (2.22).

Lemma 2.7. *Let two sectors $S^{(1)} = S_{e_1^{(1)}, e_2^{(1)}}(\alpha_1, \alpha_2)$ and $S^{(2)} = S_{e_1^{(2)}, e_2^{(2)}}(\beta_1, \beta_2)$ be given with the same assumptions as in Lemma 2.4. If we consider a function $u \in \mathcal{C}([\alpha_1, \alpha_2])$ as an element of $\mathcal{C}_R(S^{(1)})$ we get*

$$v(r, \phi) := (\overline{\mathcal{K}}_{S^{(1)}} u)(r, \phi) \in C_R(S^{(2)}),$$

this mapping is continuous between $\mathcal{C}([\alpha_1, \alpha_2])$ and $C_R(S^{(2)})$ and $v(r, \phi) = v(1, \phi)$.

Proof. We keep the notations (2.18), (2.19) and (2.20) from the proof of Lemma 2.4 and get

$$(\overline{\mathcal{K}}_{S^{(1)}} u)(r, \phi) = \frac{1}{\pi} \int_{\alpha_1}^{\alpha_2} \int_0^\infty \frac{\nu^2 a(\phi') b(\phi)}{(\nu^2 - 2\nu c(\phi', \phi) + 1)^2} u(\phi') d\nu d\phi'.$$

Using the partial fraction decomposition of

$$\frac{\nu^2}{(\nu^2 - 2\nu c(\phi', \phi) + 1)^2}$$

we get

$$\begin{aligned} & \int_0^\infty \frac{\nu^2}{(\nu^2 - 2\nu c(\phi', \phi) + 1)^2} d\nu \\ &= \frac{1}{4} \left(\frac{2c(\phi', \phi)}{1 - c(\phi', \phi)^2} + \frac{1}{(1 - c(\phi', \phi)^2)^{\frac{3}{2}}} \left(\pi + 2 \arctan \left(\frac{c(\phi', \phi)}{\sqrt{1 - c(\phi', \phi)^2}} \right) \right) \right) \end{aligned}$$

where we use the following branch of the arctan function

$$\arctan : (-\infty, \infty) \longrightarrow (-\pi/2, \pi/2).$$

So we get

$$\begin{aligned} (\overline{\mathcal{K}}_{S^{(1)}} u)(r, \phi) &= (\overline{\mathcal{K}}_{S^{(1)}} u)(1, \phi) \\ &= \frac{1}{4\pi} \int_{\alpha_1}^{\alpha_2} a(\phi') b(\phi) \left(\frac{2c(\phi', \phi)}{1 - c(\phi', \phi)^2} \right. \\ &\quad \left. + \frac{1}{(1 - c(\phi', \phi)^2)^{3/2}} \left(\pi + 2 \arctan \left(\frac{c(\phi', \phi)}{\sqrt{1 - c(\phi', \phi)^2}} \right) \right) \right) u(\phi') d\phi'. \end{aligned}$$

If $c(\phi', \phi) \in [-1, 1)$, for all $(\phi', \phi) \in [\alpha_1, \alpha_2] \times [\beta_1, \beta_2]$, we get $(\overline{\mathcal{K}}_{S^{(1)}} u)(1, \phi) \in \mathcal{C}^\infty([\beta_1, \beta_2])$. This is the case if $S^{(1)}$ and $S^{(2)}$ have no common edge. So we have proved everything in the case that $S^{(1)} \cap S^{(2)} = \{0\}$ holds. If $S^{(1)}$ and $S^{(2)}$ have a common edge we will assume that

$$S^{(1)} \cap S^{(2)} = \{\lambda e_1^{(1)} \mid \lambda \geq 0\} = \{\lambda e_1^{(2)} \mid \lambda \geq 0\}.$$

This also implies $\alpha_1 = \beta_1 = 0$. We get

$$\begin{aligned} a(\phi') &= \cos(\phi') e_1^{(1)} \cdot n^{(2)} + \sin(\phi') e_2^{(1)} \cdot n^{(2)} \\ &= \sin(\phi') e_2^{(1)} \cdot n^{(2)} \\ b(\phi) &= \cos(\phi) e_1^{(2)} \cdot n^{(1)} + \sin(\phi) e_2^{(2)} \cdot n^{(1)} \\ &= \sin(\phi) e_2^{(2)} \cdot n^{(1)} \\ c(\phi', \phi) &= (\cos(\phi) e_1^{(2)} + \sin(\phi) e_2^{(2)}) (\cos(\phi') e_1^{(1)} + \sin(\phi') e_2^{(1)}) \\ &= \cos(\phi) \cos(\phi') + \sin(\phi) \sin(\phi') e_2^{(1)} \cdot e_2^{(2)}. \end{aligned}$$

By a Taylor series expansion and using the notation $\gamma := e_2^{(1)} \cdot e_2^{(2)} \in (-1, 1)$, otherwise $S^{(1)}$ and $S^{(2)}$ would not ‘see’ each other, we get

$$\begin{aligned} 1 - c(\phi, \phi')^2 &= (\phi, \phi') \begin{pmatrix} 1 & \gamma \\ \gamma & 1 \end{pmatrix} \begin{pmatrix} \phi \\ \phi' \end{pmatrix} + O\left(\left\| \begin{pmatrix} \phi \\ \phi' \end{pmatrix} \right\|^3\right) \\ &\geq \frac{(1 - |\gamma|)}{2} (\phi^2 + (\phi')^2), \end{aligned}$$

if $\|(\phi, \phi')^T\| \leq \delta$, $\delta > 0$ sufficiently small, but we can assume that $\alpha_2, \beta_2 < \delta$ because, for greater values, the kernel is infinitely smooth. Now we get

$$\begin{aligned} |(\overline{\mathcal{K}}_{S^{(1)}} u)(r, \phi)| &\leq \frac{c_1}{4\pi} \int_0^{\alpha_2} \frac{\phi \phi'}{(\phi^2 + (\phi')^2)^{3/2}} [u(\phi')] d\phi' \\ (2.23) \qquad &\leq \|u\|_{L^\infty(S^{(1)})} \frac{c_1}{4\pi} \int_0^\infty \frac{\phi/\phi'}{(1 + (\phi/\phi')^2)^{3/2}} \frac{d\phi'}{\phi'} \\ &= \|u\|_{L^\infty(S^{(1)})} \frac{c_1}{4\pi} \int_0^\infty \frac{1}{(1 + \nu^2)^{3/2}} d\nu \\ &\leq c_2 \|u\|_{L^\infty(S^{(1)})}, \end{aligned}$$

with constants $c_1, c_2 > 0$ which depend only on α_2 and β_2 . This shows the boundedness as a mapping into $L^\infty([\beta_1, \beta_2])$. The continuity in the interior (β_1, β_2) is clear because of the smoothness of the kernel. The property

$$\lim_{\phi \rightarrow 0} (\overline{\mathcal{K}}_{S^{(1)}} u)(1, \phi) = (\overline{\mathcal{K}}_{S^{(1)}} u(0))(1, 0)$$

follows similar to the proof of the corresponding property of Mellin convolution operators. \square

Remark 2.8. Formula (2.23) and the theory developed by Elschner in [8] show that much more is true than $\mathcal{K}_{S^{(1)}} u \in \mathcal{C}_R(S^{(2)})$. It follows that the mapping $\mathcal{K}_{S^{(1)}}$ is continuous for a scale of weighted L^2 spaces. But we will not need this result here.

A more geometric proof of Lemma 2.7 can be given with the help of Lemma 2.4. The above proof has the advantage that the connection to Mellin convolution operators becomes clear.

This lemma is used to prove:

Lemma 2.9. *Let again the two sectors $S^{(1)} = S_{e_1^{(1)}, e_2^{(1)}}(\alpha_1, \alpha_2)$ and $S^{(2)} = S_{e_1^{(2)}, e_2^{(2)}}(\beta_1, \beta_2)$ be given as in Lemma 2.4. Then the mapping*

$$\bar{\mathcal{K}}_{S^{(1)}} : \mathcal{C}_R(S^{(1)}) \longrightarrow \mathcal{C}_R(S^{(2)})$$

is continuous.

Proof. Let $u \in \mathcal{C}_R(S^{(1)})$. Define

$$u_0(\phi) := u(0, \phi) \in \mathcal{C}([\alpha_1, \alpha_2]).$$

Then $u_1(r, \phi) := u(r, \phi) - u_0(\phi) \in \mathcal{C}_R(S^{(1)})$, and we get for all $\varepsilon > 0$, $\delta = \delta(\varepsilon) > 0$ such that

$$|u_1(r, \phi)| \leq \varepsilon, \quad (r, \phi) \in [0, \delta] \times [\alpha_1, \alpha_2].$$

Because of Lemma 2.7, we know that

$$(\bar{\mathcal{K}}_{S^{(1)}} u_0)(r, \phi) \in \mathcal{C}_R(S^{(2)})$$

and

$$\begin{aligned} \|\bar{\mathcal{K}}_{S^{(1)}} u_0\|_{L^\infty(S^{(2)})} &\leq c_1 \|u_0\|_{L^\infty(S^{(1)})} \\ &\leq c_1 \|u\|_{L^\infty(S^{(1)})}, \quad c_1 > 0. \end{aligned}$$

So we only have to prove

$$(\bar{\mathcal{K}}_{S^{(1)}} u_1) \in \mathcal{C}_R(S^{(2)})$$

and

$$\|\bar{\mathcal{K}}_{S^{(1)}} u_1\|_{L^\infty(S^{(2)})} \leq c_2 \|u\|_{L^\infty(S^{(1)})}.$$

First we repeat

$$\begin{aligned} &(\bar{\mathcal{K}}_{S^{(1)}} u_1)(r, \phi) \\ &= \frac{1}{\pi} \int_{\alpha_1}^{\alpha_2} \int_0^\infty \frac{r(r')^2 a(\phi') b(\phi)}{(r^2 - 2rr'c(\phi', \phi) + (r')^2)^2} u_1(r', \phi) dr' d\phi', \end{aligned}$$

where a , b and c are defined in (2.18), (2.19) and (2.20). Because of

$$\frac{1}{\pi} \int_{\alpha_1}^{\alpha_2} \int_0^\infty \frac{r(r')^2 |a(\phi')| |b(\phi)|}{(r^2 - 2rr'c(\phi', \phi) + (r')^2)^2} dr' d\phi' =: c_2 < \infty,$$

see Lemma 2.7, we can conclude that $\overline{\mathcal{K}}_{S^{(1)}} u_1$ is well defined and

$$\|\overline{\mathcal{K}}_{S^{(1)}} u_1\|_{L^\infty(S^{(2)})} \leq c_3 \|u_1\|_{L^\infty(S^{(1)})}.$$

We prove

$$\lim_{r \searrow 0} (\overline{\mathcal{K}}_{S^{(1)}} u_1)(r, \phi) = 0,$$

uniformly in $\phi \in [\beta_1, \beta_2]$, which proves the continuity for $r = 0$. But, given an $\varepsilon > 0$, we find $\delta > 0$ such that

$$|u_1(r, \phi)| < \varepsilon, \quad r < \delta.$$

Now we can estimate

$$\begin{aligned} & |(\overline{\mathcal{K}}_{S^{(1)}} u_1)(r, \phi)| \\ & \leq \frac{1}{\pi} \int_{\alpha_1}^{\alpha_2} \int_0^\delta \frac{r(r')^2 |a(\phi')| |b(\phi)|}{(r^2 - 2rr'c(\phi', \phi) + (r')^2)^2} |u_1(r', \phi')| dr' d\phi' \\ & \quad + \frac{1}{\pi} \int_{\alpha_1}^{\alpha_2} \int_\delta^\infty \frac{r(r')^2 |a(\phi')| |b(\phi)|}{(r^2 - 2rr'c(\phi', \phi) + (r')^2)^2} |u_1(r', \phi')| dr' d\phi' \\ & \leq \frac{\varepsilon}{\pi} \int_{\alpha_1}^{\alpha_2} \int_0^\delta \frac{r(r')^2 |a(\phi')| |b(\phi)|}{(r^2 - 2rr'c(\phi', \phi) + (r')^2)^2} dr' d\phi' \\ & \quad + \frac{\|u_1\|_{L^\infty(S^{(1)})}}{\pi} \int_{\alpha_1}^{\alpha_2} \int_\delta^\infty \frac{r(r')^2 |a(\phi')| |b(\phi)|}{(r^2 - 2rr'c(\phi', \phi) + (r')^2)^2} dr' d\phi' \\ & \leq c_2 \varepsilon + \frac{\|u_1\|_{L^\infty(S^{(1)})}}{\pi} \int_{\alpha_1}^{\alpha_2} \int_\delta^\infty \frac{r(r')^2 |a(\phi')| |b(\phi)|}{(r^2 - 2rr'c(\phi', \phi) + (r')^2)^2} dr' d\phi'. \end{aligned}$$

But

$$\begin{aligned} & \int_{\alpha_1}^{\alpha_2} \int_\delta^\infty \frac{r(r')^2 |a(\phi')| |b(\phi)|}{(r^2 - 2rr'c(\phi', \phi) + (r')^2)^2} dr' d\phi' \\ & = \int_{\alpha_1}^{\alpha_2} |a(\phi')| |b(\phi)| \frac{1}{r} \int_\delta^\infty \frac{(r'/r)^2}{(1 - 2r'/rc(\phi', \phi) + (r'/r)^2)^2} dr' d\phi' \\ & = \int_{\alpha_1}^{\alpha_2} |a(\phi')| |b(\phi)| \int_{\delta/r}^\infty \frac{\nu^2}{(1 - 2\nu c(\phi', \phi) + \nu^2)^2} d\nu d\phi' \\ & \leq \int_{\alpha_1}^{\alpha_2} \int_{\delta/r}^\infty \frac{\nu^2}{(1 - 2\nu + \nu^2)^2} d\nu d\phi', \quad \text{if } r < \delta, \\ & \leq (\alpha_2 - \alpha_1) \int_{\delta/r}^\infty \frac{\nu^2}{(1 - 2\nu + \nu^2)^2} d\nu, \quad r \searrow 0, \end{aligned}$$

uniformly in ϕ . So we have proved

$$\lim_{r \searrow 0} (\overline{\mathcal{K}}_{S^{(1)}} u_1)(r, \phi) = 0$$

uniformly in $\phi \in [\beta_1, \beta_2]$. This shows the continuity for all points $(0, \phi)^T$, $\phi \in [\beta_1, \beta_2]$.

It remains to prove the continuity along the common edges of two triangles. Let the edge be given by $L = \{(0, 0, t) \mid t \geq 0\}$ and denote by α the angle enclosed by $S^{(1)}$ and $S^{(2)}$. We further introduce the half plane $E^{(1)}$ which is the extension of the triangle $S^{(1)}$; this means that if $S^{(1)}$ is contained in $\{(x, 0, z) \mid x \geq 0, z \in \mathbf{R}\}$, then $E^{(1)} = \{(x, 0, z) \mid x \geq 0, z \in \mathbf{R}\}$. For $\bar{x} \in L$ and $x_n \in S^{(2)}$, $\lim_{n \rightarrow \infty} x_n = \bar{x}$, we get

$$\lim_{n \rightarrow \infty} (\mathcal{K}_{S^{(1)}} u)(x_n) = \frac{u(\bar{x})}{2} (1 + \cos(\alpha)),$$

because of (2.21) we get

$$\begin{aligned} & \left| (\mathcal{K}_{S^{(1)}} u)(x_n) - \frac{u(\bar{x})}{2} (1 + \cos(\alpha)) \right| \\ &= |(\mathcal{K}_{S^{(1)}} u)(x_n) - (\mathcal{K}_{E^{(1)}} u(\bar{x}))(x_n)| \\ &= |(\mathcal{K}_{S^{(1)}} [u(\cdot) - u(\bar{x})])(x_n) - (\mathcal{K}_{E^{(1)} \setminus S^{(1)}} u(\bar{x}))(x_n)|. \end{aligned}$$

For $\delta > 0$ define $\tilde{S}_\delta^{(1)} := B_\delta(\bar{x}) \cap S^{(1)}$, and we get

$$\begin{aligned} & \left| (\mathcal{K}_{S^{(1)}} u)(x_n) - \frac{u(\bar{x})}{2} (1 + \cos(\alpha)) \right| \\ & \leq \sup_{x \in \tilde{S}_\delta^{(1)}} |u(x) - u(\bar{x})| \sigma_{x_n, n^{(2)}}(S^{(1)}) + 2 \|u\|_{L^\infty(S^{(1)})} \sigma_{x_n, n^{(2)}}(S^{(1)} \setminus \tilde{S}_\delta^{(1)}) \\ & \quad + |u(\bar{x})| \sigma_{x_n, n^{(2)}}(E^{(1)} \setminus S^{(1)}) \end{aligned}$$

The first term can be made arbitrarily small by choosing δ sufficiently small. The two other terms go to zero with $n \rightarrow \infty$ because the projected areas are getting smaller and smaller as the point x_n approaches the plane $E^{(1)}$, see the definition of $\sigma_{x_n, n^{(2)}}$ in formula (2.14). So we proved the continuity of $\mathcal{K}_{S^{(1)}} u$ on the edge, the proof of the continuity in the neighborhood follows by similar arguments. \square

Now we know that $\mathcal{K}_S : C_R(S^{(1)} \cup S^{(2)}) \mapsto C_R(S^{(1)} \cup S^{(2)})$ is well defined and continuous by (2.4). Before we start to apply this result to the general situation $C_R(S)$, given by (2.1), we might ask the question if the special case of only two sectors was responsible for the fact that \mathcal{K}_S does not map continuous functions on continuous functions. So the mapping properties of \mathcal{K}_S might be better if S is the boundary of a closed bounded domain in \mathbf{R}^3 . The following definition is necessary to describe the neighborhood of a vertex of S .

Definition 2.10. A closed spherical polygon $\gamma \subset S^2 := \{(x, y, z)^T \in \mathbf{R}^3 \mid x^2 + y^2 + z^2 = 1\}$ is defined by m vertices $\gamma_i \in S^2$, $i = 0(1)m - 1$, $\gamma_m := \gamma_0$ and

$$(2.24) \quad \gamma := \bigcup_{j=0}^{m-1} \widehat{\gamma_j, \gamma_{j+1}},$$

where $\widehat{\gamma_j, \gamma_{j+1}}$ is the shorter of the two great circles connecting γ_j and γ_{j+1} . We further assume that none of the $\widehat{\gamma_j, \gamma_{j+1}}$ intersect each other in their relative interior and that the γ_j are given in such a way that there is always a short and a long connecting great circle. Connected to γ is the infinite *polyhedral cone* Γ

$$(2.25) \quad \Gamma := \{rx \mid r \geq 0, x \in \gamma\},$$

$$\Gamma = \bigcup_{j=0}^{m-1} \Gamma_j$$

$$(2.26) \quad \Gamma_j := \{rx \mid r \geq 0, x \in \widehat{\gamma_j, \gamma_{j+1}}\}.$$

The next lemma states the fact that, even for the boundary S of a closed domain, the operator \mathcal{K}_S does not map the space $\mathcal{C}(S)$ or $\mathcal{C}_P(S)$ into itself.

Lemma 2.11. Consider a spherical polygon $\gamma = \cup_{j=0}^{m-1} \gamma_j$ according to Definition 2.10 and the corresponding cone $\Gamma = \cup_{j=0}^{m-1} \Gamma_j$. For every sector Γ_j a normal n_j is chosen and we consider $S = \Gamma$ as our surface where the reflection operator \mathcal{K}_S is defined. For simplicity, we will also assume that the reflectivity function is equal to 1. In general we have

$$\mathcal{K}_S : \mathcal{C}(S) \not\mapsto \mathcal{C}_P(S).$$

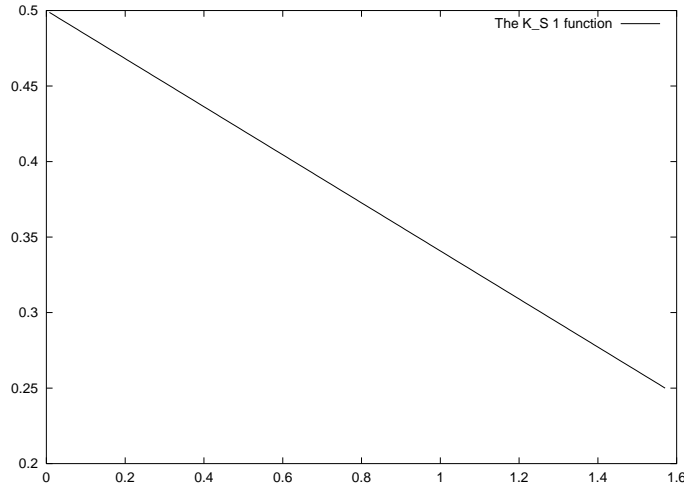


FIGURE 2.3. The function $(\mathcal{K}_S \mathbf{1})((\cos(\phi), 0, \sin(\phi))^T)$.

Proof. Again it is sufficient to consider an example. The example relies on the visibility function which essentially brings us to the situation of Corollary 2.6. We choose $m = 4$, $\gamma_0 = (0, 1, 0)^T$, $\gamma_1 = (1, 0, 0)^T$, $\gamma_2 = (0, 0, 1)^T$, $\gamma_3 = 1/\sqrt{2}(0, -1, -1)^T$ and the normals $n_0 = (0, 0, 1)^T$, $n_1 = (0, 1, 0)^T$, $n_2 = n_3 = (-1, 0, 0)^T$. Then the surface Γ_1 can only see Γ_0 , and for $x \in \Gamma_1$ we get

$$(\mathcal{K}_S u)(x) = (\overline{\mathcal{K}}_{\Gamma_0} u)(x),$$

$u \in \mathcal{C}(S)$. Now we choose $u \equiv 1$ and get the picture in Figure 2.3 for $(\mathcal{K}_S \mathbf{1})(r(\cos(\phi), 0, \sin(\phi))^T) = (\mathcal{K}_S \mathbf{1})((\cos(\phi), 0, \sin(\phi))^T)$. Because this function is independent of r , we see again that the function is not continuous near the origin. \square

The example in Lemma 2.11 can be modified to prove the same result for a closed bounded domain. The cone in the above lemma was the boundary of a nonconvex set. The last possibility to improve the mapping properties of the operator \mathcal{K}_S would be to restrict our consideration to the boundaries S of convex sets. Here the mapping properties of \mathcal{K}_S change. We will give this result, which can be proved by geometrical considerations, in the following remark.

Remark 2.12. If we examine the proof of Lemma 2.4 and Lemma 2.9 we notice that it is enough to show that the image $\mathcal{K}_\Gamma \mathbf{1}$ of the constant function $\mathbf{1}$ is continuous near the peak of the cone Γ . So we must show

$$\mathcal{K}_\Gamma \mathbf{1} \in \mathcal{C}_P(\Gamma).$$

We already know that $(\mathcal{K}_\Gamma \mathbf{1})|_{\Gamma_j}$ is independent of the radial variable. So we must get the result $(\mathcal{K}_\Gamma \mathbf{1})|_{\Gamma_j} \equiv \text{const}$.

If the cone $\Gamma = \cup_{j=0}^{m-1} \Gamma_j$ is the boundary of a convex set Ω and, if all normals n_j point into the interior of Ω , we get for $x \in \Gamma_0$ (we choose Γ_0 without any restriction)

$$\sigma_{x,n_0} \left(\bigcup_{j=2}^{m-1} \Gamma_j \right) = \sigma_{x,n_0} \left(\bigcup_{j=2}^{m-1} E_j \right),$$

where the plane E_j is generated by Γ_j and has the same normal n_j . Here we have used the convexity because the cone is the intersection of the bounding half spaces and the visibility function is equal to 1, so the above σ is equal to the operator \mathcal{K}_Γ applied to the $\mathbf{1}$ function. If we assume that E_j has the two basis vectors $g_1^{(j)}$ and $g_2^{(j)}$, we get (see Definition 2.3)

$$\begin{aligned} P(E_j) &= \{y \in S_{n,\varepsilon}^2(x) \mid \exists \lambda \geq 0 : x + \lambda(y - x) \in \langle g_1^{(j)}, g_2^{(j)} \rangle\} \\ &= x + \{y \in S_{n,\varepsilon}^2(0) \mid y \cdot n_j \leq 0\}, \end{aligned}$$

which is independent of $x \in \Gamma_0$. So we get

$$\sigma_{x,n_0} \left(\bigcup_{j=2}^{m-1} \Gamma_j \right) = \frac{\mu(\cup_{j=2}^{m-1} P_\perp(E_j))}{\pi\varepsilon^2}$$

which is independent of x .

So we get in the case of a convex cone Γ

$$\mathcal{K}_\Gamma : \mathcal{C}(\Gamma) \longrightarrow \mathcal{C}_P(\Gamma).$$

Again simple examples show that

$$\mathcal{K}_\Gamma : \mathcal{C}(\Gamma) \longrightarrow \mathcal{C}(\Gamma)$$

is not true in general.

After we have excluded the space $\mathcal{C}_P(S)$ as a candidate for an existence theory, we consider only the space $\mathcal{C}_R(S)$ in the following. To show

$$(2.27) \quad \mathcal{K}_S : \mathcal{C}_R(S) \mapsto \mathcal{C}_R(S)$$

we will localize the operator by a partition of the unity around each corner. Then we use Lemma 2.9, but we must take care of the influence of local shadows. This will be done in the following discussion.

Let the surface S be given according to (2.1), with normal vectors n_j , $j = 1(1)n$. We denote by $\{x_k \mid k = 1(1)m\}$ the vertices of S , and we assume that we have given a partition of unity on S of the following form. There are m functions $\varphi_k : S \rightarrow \mathbf{R}_0^+$, such that

$$(2.28) \quad \left. \begin{array}{l} \varphi_k \mid \Delta_j \in \mathcal{C}^\infty(\Delta_j), \quad j = 1(1)n, \\ \sum_{k=1}^m \varphi_k(x) = 1, \quad x \in S. \end{array} \right\}$$

We can construct the function φ_k in such a way that

$$\varphi_k \mid \Delta_j = 0 \quad \text{if } x_k \notin \Delta_j,$$

and if $x_k \in \Delta_j$ and $y \in \Delta_j$ is one of the other vertices of Δ_j , then there exists a neighborhood U of y in Δ_j such that

$$\begin{aligned} \varphi_k \mid U &\equiv 0 \quad \text{and} \\ \varphi_k \mid W &\equiv 1, \end{aligned}$$

for a neighborhood W of x_k in Δ_j . We remark here that it is sufficient to construct such functions φ_k on every triangle Δ_j .

To prove (2.27) we can restrict our considerations to a neighborhood of a vertex. This follows with the help of the partition of unity from above. Let $u \in \mathcal{C}_R(S)$

$$(\mathcal{K}_S u) = (\mathcal{K}_S \varphi_k u) + \mathcal{K}_S \left(\sum_{\substack{j=1 \\ j \neq k}}^m \varphi_j u \right).$$

There is an $\varepsilon > 0$ such that $U_\varepsilon(x_k) \cap \text{supp}(\varphi_j) = \emptyset$, $j = 1(1)m$, $j \neq k$. So we know that

$$\mathcal{K}_S \left(\sum_{\substack{j=1 \\ j \neq k}}^m \varphi_j u \right) \Big|_{U_\varepsilon(x_k) \cap S}$$

is Lipschitz continuous with respect to the usual Euclidean norm on S , see [10]. From now on we assume $x_k = 0$ and, by $\Delta_{i_1}, \dots, \Delta_{i_l}$, we denote all triangles such that $0 \in \Delta_{i_j}$. Let

$$\begin{aligned} \tilde{\Delta}_j &:= \{rx \mid r \geq 0, x \in \Delta_{i_j}\}, \\ \tilde{S} &:= \bigcup_{j=1}^l \tilde{\Delta}_j. \end{aligned}$$

This implies

$$(\mathcal{K}_S \varphi_k u)(x) = (\mathcal{K}_{\tilde{S}} \varphi_k u)(x), \quad x \in U_\varepsilon(0) \cap S.$$

So it is enough to study the image $\mathcal{K}_{\tilde{S}} u$ on \tilde{S} , $u \in \mathcal{C}_R(\tilde{S})$. Now we pick two arbitrary faces, $\tilde{\Delta}_1$ and $\tilde{\Delta}_2$ for example and it is clear that it is enough to prove

$$(2.29) \quad \int_{\tilde{\Delta}_2} V(x, y) \frac{[n_{i_1} \cdot (y-x)][n_{i_2} \cdot (x-y)]}{\|x-y\|^4} u(y) ds_y \in \mathcal{C}_R(\tilde{\Delta}_1).$$

Here V is the visibility function of \tilde{S} , but for $x \in U_\varepsilon(0) \cap S$ and $y \in \text{supp}(\varphi_k)$ this is equal to the visibility function on S . The proof of (2.29) is sufficient because of

$$(\mathcal{K}_{\tilde{S}} u)(x) = \frac{\rho_1}{\pi} \sum_{j=1}^l \int_{\tilde{\Delta}_j} V(x, y) \frac{[n_{i_1} \cdot (y-x)][n_{i_j} \cdot (x-y)]}{\|x-y\|^4} u(y) ds_y.$$

Next we assume that $\tilde{\Delta}_1 = S^{(2)}$ and $\tilde{\Delta}_2 = S^{(1)}$ are given by sectors $S^{(1)} = S_{e_1^{(1)}, e_2^{(1)}}(\alpha_1, \alpha_2)$ and $S^{(2)} = S_{e_1^{(2)}, e_2^{(2)}}(\beta_1, \beta_2)$, according to Lemma 2.4. This allows us to write the integral in (2.29) for $x = x(r, \phi)$, $r \geq 0$, $\phi \in [\beta_1, \beta_2]$, in the following form

$$\sum_{j=1}^{\alpha(x)} \int_{\alpha_j^{(1)}(\phi)}^{\alpha_j^{(2)}(\phi)} \int_0^\infty \frac{rr' a(\phi') b(\phi)}{(r^2 - 2rr' c(\phi', \phi) + (r')^2)^2} u(r', \phi') dr' d\phi',$$

where the functions a, b and c were defined in (2.18)–(2.20). We further have

$$\alpha_1 \leq \alpha_1^{(1)}(x) \leq \alpha_1^{(2)}(x) \leq \alpha_2^{(1)} \cdots \leq \alpha_{o(x)}^{(2)} \leq \alpha_2,$$

and remark that these functions are not unique, but we can assume this local representation of the visible part of $S^{(2)}$, because the edges of all other faces $\tilde{\Delta}_j$, $j = 3(1)l$, are rays emanating from 0. If there are no other faces between $S^{(1)}$ and $S^{(2)}$, this means no shadows, we get $o(x) = 1$ and $\alpha_1^{(1)}(x) \equiv \alpha_1$, $\alpha_1^{(2)} \equiv \alpha_2$ and Lemma 2.9 proves (2.29).

In the general case we divide the function u into two parts

$$\begin{aligned} u(r', \phi') &= u_0(\phi') + u_1(r', \phi'), \\ u_0(\phi') &:= u(0, \phi'), \\ u_1(r', \phi') &:= u(r', \phi') - u_0(\phi'), \end{aligned}$$

as we have done it in the proof of Lemma 2.9. Every summand in the above formula can now be split in the following way, $j \in \{1, \dots, o(x)\}$,

$$\begin{aligned} &\int_{\alpha_j^{(1)}(\phi)}^{\alpha_j^{(2)}(\phi)} \frac{rr'a(\phi')b(\phi)}{(r^2 - 2rr'c(\phi', \phi) + (r')^2)^2} u(r', \phi') dr' d\phi' \\ &= \int_{\alpha_j^{(1)}(\phi)}^{\alpha_1^{(2)}(\phi)} \frac{rr'a(\phi')b(\phi)}{(r^2 - 2rr'c(\phi', \phi) + (r')^2)^2} u_1(r', \phi') dr' d\phi' \\ &\quad + \int_{\alpha_j^{(1)}(\phi)}^{\alpha_j^{(2)}(\phi)} \frac{rr'a(\phi')b(\phi)}{(r^2 - 2rr'c(\phi', \phi) + (r')^2)^2} u_0(\phi') dr' d\phi' \\ &=: f_1(r, \phi) + f_0(\phi). \end{aligned}$$

The continuity of $f_1(r, \phi)$ follows analogously to the proof of Lemma 2.9; here it is only important that we can find for any given $\delta > 0$ a positive $r_0 > 0$ such that

$$|u_1(r, \phi)| \leq \delta \quad \text{if } \phi \in [\alpha_1, \alpha_2], \quad r \leq r_0.$$

The dependence of the integral boundaries on ϕ , which has not appeared in the proof of Lemma 2.9, can be treated by a splitting which we introduce in formula (2.30). The only property which remains to prove is the continuity of $f_0(\phi)$.

Using again the functions a , b and c introduced in (2.18)–(2.20), we define

$$\begin{aligned} \kappa(\phi, \phi') := & a(\phi')b(\phi) \left(\frac{2c(\phi', \phi)}{1 - c(\phi', \phi)^2} \right. \\ & \left. + \frac{1}{(1 - c(\phi', \phi)^2)^{3/2}} \left(\pi + 2 \arctan \left(\frac{c(\phi', \phi)}{\sqrt{1 - c(\phi', \phi)^2}} \right) \right) \right) \end{aligned}$$

and get (see Lemma 2.7)

$$f_0(\phi) = \int_{\alpha_j^{(1)}(\phi)}^{\alpha_j^{(2)}(\phi)} \kappa(\phi, \phi') u_0(\phi') d\phi'.$$

First we assume that $S^{(1)}$ and $S^{(2)}$ have no common edge. Then $\kappa(\phi, \phi')$ is a C^∞ function in both variables and bounded from above. So the smoothness of $\alpha_j^{(1)}$ and $\alpha_j^{(2)}$ determines the smoothness of f_0 . This shows that f_0 is a Lipschitz continuous function.

If $S^{(1)}$ and $S^{(2)}$ have a common edge, we assume that this edge is given by $\phi = 0 = \phi'$. But there are only finitely many faces $\tilde{\Delta}_j$, $j = 2(1)l$, which create the shadows. So we can assume that for ϕ and ϕ' small enough there is no shadow. This means $V(x(r, \phi), y(r', \phi')) \equiv 1$, if $\phi, \phi' \leq \phi_0$, where $\phi_0 > 0$. Without any restriction we are now in the following situation

$$(2.30) \quad \left. \begin{aligned} \alpha_1^{(1)}(\phi) &= 0, \\ \alpha_1^{(2)}(\phi) &\geq \phi_0, \\ \alpha_k^{(1)}(\phi), \alpha_k^{(2)}(\phi) &\geq \phi_0, \quad k \geq 2. \end{aligned} \right\}$$

For the integrals of the form

$$\int_{\alpha_k^{(1)}(\phi)}^{\alpha_k^{(2)}(\phi)} \kappa(\phi, \phi') u_0(\phi') d\phi', \quad k \geq 2,$$

we can argue as in the proof of the two faces with no common edge. The integral for $k = 1$ can be written in the following way

$$\begin{aligned} \int_{\alpha_1^{(1)}(\phi)}^{\alpha_1^{(2)}(\phi)} \kappa(\phi, \phi') u_0(\phi') d\phi' &= \int_0^{\phi_0} \kappa(\phi, \phi') u_0(\phi') d\phi' \\ &+ \int_{\phi_0}^{\alpha_1^{(2)}(\phi)} \kappa(\phi, \phi') u_0(\phi') d\phi'. \end{aligned}$$

The continuity of the first summand follows from Lemma 2.9 and the continuity of the second summand follows again by the boundedness of $\kappa(\phi', \phi)$, $\phi' \geq \phi_0$. So we have proved the following theorem.

Theorem 2.13. *Let S be a surface according to (2.1) with normals n_j , $j = 1(1)n$, and a reflectivity function ρ which fulfills (2.3). Then the reflection operator \mathcal{K}_S , see (2.2), is a continuous operator in $\mathcal{C}_R(S)$.*

Using again (2.4) and the fixed point theorem of Banach one gets the final result of this section.

Theorem 2.14. *Let the surface S and the reflectivity function ρ be given according to (2.1) and (2.3). Then the radiosity equation (1.1)*

$$(I - \mathcal{K}_S)u = E, \quad E \in \mathcal{C}_R(S),$$

has a uniquely determined solution $\bar{u} \in \mathcal{C}_R(S)$.

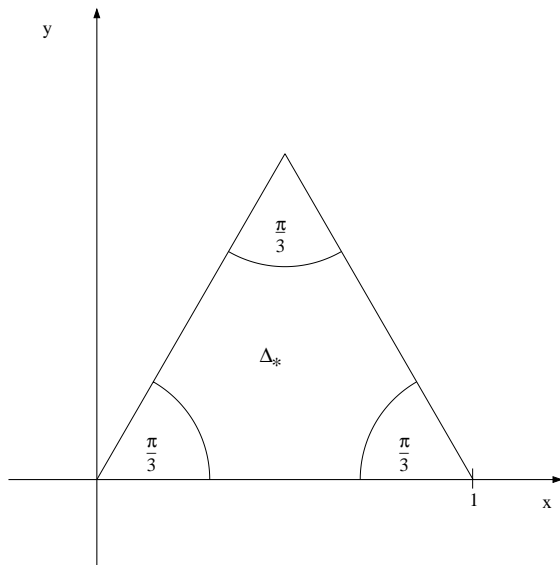
We now have a function space where we know that the solutions of the radiosity equation exist and point evaluations are possible if one does not evaluate the functions in the corners. Therefore we can formulate a collocation method for the approximate solution of the radiosity equation. Numerical examples in Section 4 will demonstrate the results of Theorems 2.13 and 2.14.

3. The collocation method for the solution of the radiosity equation. In order to formulate the collocation method for the approximate solution of the radiosity equation (1.1) on S , S given by (2.1), we first define a partition of S . It is clear that we can map every triangle Δ_j , $j \in \{1, \dots, n\}$, by an affine linear bijective mapping Ψ_j on a fixed reference triangle $\Delta_* \subset \mathbf{R}^2$,

$$(3.1) \quad \Psi_j : \Delta_j \xrightarrow{1:1} \Delta_*.$$

We choose the reference triangle shown in Figure 3.1.

The analysis of Section 2 shows that the solution of the radiosity equation will be continuous only with respect to polar coordinates near

FIGURE 3.1. The reference triangle Δ_* .

the vertices of the triangle Δ_j . We further must be able to introduce a grading of the meshes towards the edges, respectively vertices, of the triangle, see [10, 17]. For this purpose we introduce first a coarse triangulation of Δ_* of the form shown in Figure 3.2.

For each of the triangles $\Delta_{*,l}$, $l = 1(1)6$, there is an affine linear transformation κ_l , which maps $\Delta_{*,l}$ on a further reference triangle $\Delta_* = \Delta_{*,1}$. Each κ_l , $l = 1(1)6$, has the form

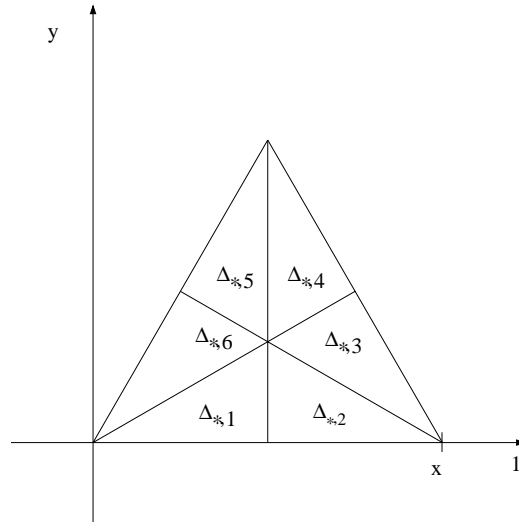
$$(3.2) \quad \kappa_l \begin{pmatrix} x \\ y \end{pmatrix} := U_l \left(\begin{pmatrix} x \\ y \end{pmatrix} - u_l \right),$$

where u_l is one of the vertices of Δ_* and U_l is an orthonormal matrix. We can further assume that the edge of $\Delta_{*,l}$, which is also an edge of Δ_* , is mapped on the lower edge $\{(x, 0) \mid 0 \leq x \leq 0.5\}$ of Δ_* . The reference triangle

$$(3.3) \quad \Delta_\bullet := \{(x, y) \mid 0 \leq x \leq 1/2, 0 \leq y \leq x \tan(\pi/6)\}$$

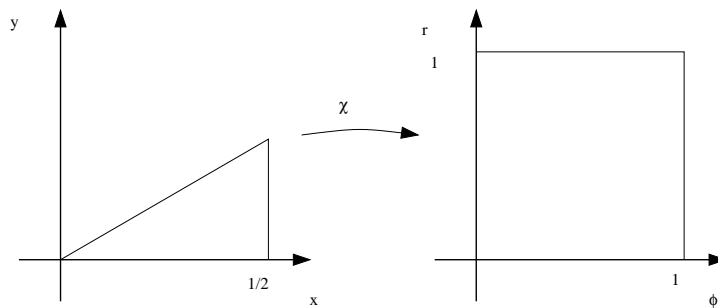
can be mapped by a nonlinear transformation χ on a reference square

$$(3.4) \quad \square := \{(x, y) \mid 0 \leq x, y \leq 1\}.$$

FIGURE 3.2. The coarse triangulation of Δ_* .

$$(3.5) \quad \begin{aligned} \begin{pmatrix} \phi \\ r \end{pmatrix} &:= \chi \begin{pmatrix} x \\ y \end{pmatrix} \\ &:= \begin{pmatrix} \frac{6}{\pi} \arctan \frac{y}{x} \\ 2x \end{pmatrix}, \quad x > 0, \end{aligned}$$

and we will never need the evaluation for $x = 0$, see Figure 3.3. We would like to mention that the function \arctan in formula (3.5) was

FIGURE 3.3 The mapping χ .

motivated by the fact that the author tried to interpret the second coordinate as a (scaled) angular coordinate. But it is clear that the function arctan and its inverse are differentiable for the interval, which we consider. So the omission of this function is possible and may lead to a simpler implementation of the collocation method.¹ If we omit the arctan function in formula (3.5) we get the Duffy transform, which is often used for the regularization of weakly singular integrals, see [18]. This is not our motivation here. The only reason at this point is the use of local polar coordinates in order to get the regularity of the solution. Now it is clear that the whole construction process for the graded mesh and the refinement can be done on \square . Here we will define meshes which are graded toward the vertices in both directions r and ϕ .

Given a grading exponent p and a natural number N we construct a partition of \square into rectangles, where the quotient of the length of the sides of the rectangles stays bounded, independent of N . First define a grid

$$(3.6) \quad \left\{ \left(\frac{i}{N} \right)^p \mid i = 0(1)N \right\} \subset [0, 1]$$

on the interval $[0, 1]$. Then we partition the L shaped region

$$(3.7) \quad L_{N,p,i} = \left\{ (x, y) \in \square \mid \min\{x, y\} \in \left[\left(\frac{i}{N} \right)^p, \left(\frac{i+1}{N} \right)^p \right] \right\}, \quad i = 0(1)N-1,$$

by first introducing the square

$$\left[\left(\frac{i}{N} \right)^p, \left(\frac{i+1}{N} \right)^p \right]^2$$

and then the rectangles

$$\left[\left(\frac{i+1}{N} \right)^p, 1 \right] \times \left[\left(\frac{i}{N} \right)^p, \left(\frac{i+1}{N} \right)^p \right]$$

and

$$\left[\left(\frac{i}{N} \right)^p, \left(\frac{i+1}{N} \right)^p \right] \times \left[\left(\frac{i+1}{N} \right)^p, 1 \right]$$

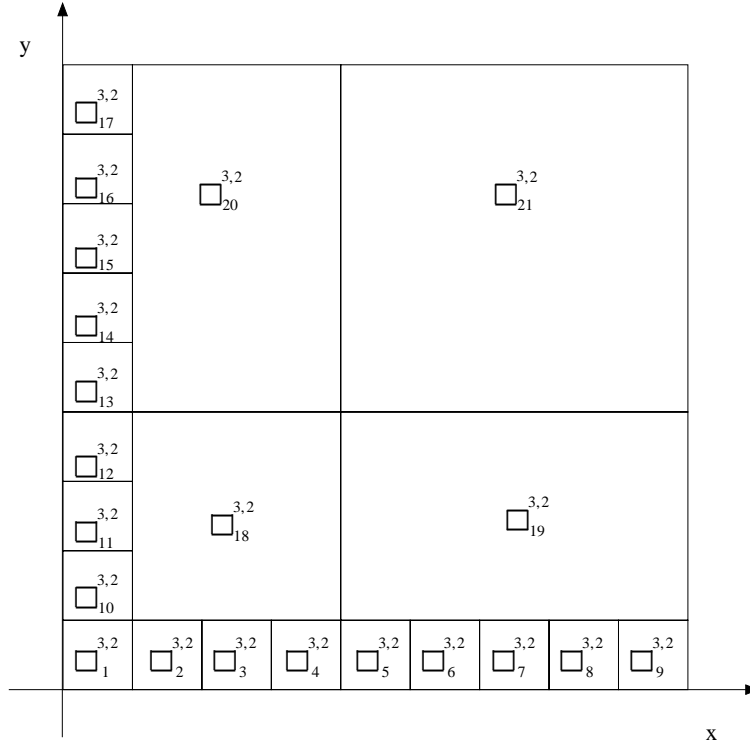


FIGURE 3.4. The partition $\wp_{3,2}$ of \square .

are divided into small rectangles, where the quotient between the side lengths is kept close to 1, see Figure 3.4. Therefore we choose

$$\begin{aligned}
 \nu_{N,p,i} &:= 1 + \left\lceil \frac{1 - (i + 1/N)^p}{(i + 1/N)^p - (i/N)^p} \right\rceil, \quad i = 0(1)N - 1, \\
 (3.8) \quad &\leq C \frac{N^p}{(i + 1)^{p-1}}
 \end{aligned}$$

rectangles in $L_{N,p,i}$. This results in

$$(3.9) \quad \nu_{N,p} := \sum_{i=1}^N \nu_{N,p,i}$$

rectangles $\square_j^{N,p}$, $j = 1(1)\nu_{N,p}$, which cover \square . We assume that the rectangles are numbered according to Figure 3.4.

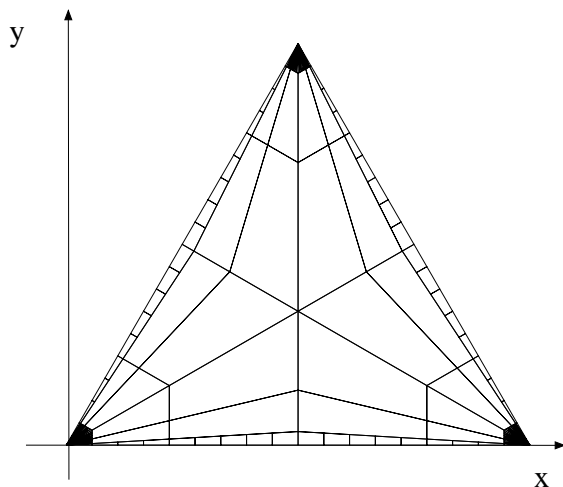


FIGURE 3.5. The partition of Δ_* if $\wp_{3,2}$ is used for all sub triangles.

Each $\square_j^{N,p}$, $j = 1(1)\nu_{N,p}$, is itself the image of \square under a linear affine mapping $\tau_j^{N,p}$,

$$(3.10) \quad \tau_j^{N,p} : \square \longrightarrow \square_j^{N,p}.$$

The partition $\wp_{N,p} := \{\square_j^{N,p} \mid j = 1(1)\nu_{N,p}\}$ can now be mapped on one $\Delta_{*,l}$. If we choose the above partition of \square for all $\Delta_{*,l}$, $l = 1(1)6$, we get the partition of Δ_* shown in Figure 3.5.

Formulas (3.8) and (3.9) show that

$$(3.11) \quad \nu_{N,p} \leq C \begin{cases} N^2 & p \in [1, 2), \\ \ln(N)N^2 & p = 2, \\ N^p & p > 2, \end{cases}$$

$C > 0$, a constant independent of N .

Now it is clear that we can construct a partition of S , given three grading exponents $(p_1^{(j)}, p_2^{(j)}, p_3^{(j)})$ for every triangle Δ_j , where $p_i^{(j)}$ determines the grading towards edge i of Δ_j . Further we need a number N . In principle, we can choose six grading exponents for every triangle and also N can depend on every sub triangle of Δ_j (this may be useful

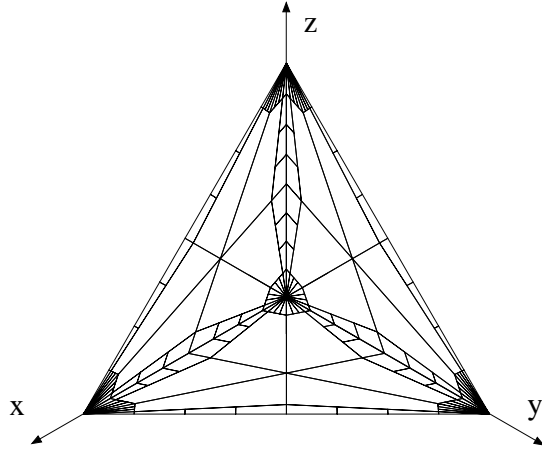


FIGURE 3.6. The partition of $S^{(1)}$, using $\varphi_{2,2}$ for every sub triangle.

in practice). But for simplicity we will only use one number N in our examples. The number ν_N of all elements of our partition is then given by

$$(3.12) \quad \nu_N := \sum_{j=1}^n 2 \sum_{i=1}^3 \nu_{N,p_i^{(j)}} = O_{N \rightarrow \infty}(\nu_{N,p^*}),$$

where p^* is the maximal grading exponent.

As an example we consider the following very simple surface $S^{(1)}$

$$(3.13) \quad S^{(1)} := \Delta_1^{(1)} \cup \Delta_2^{(1)} \cup \Delta_3^{(1)}$$

where the triangles are defined by

	vertices			normal
$\Delta_1^{(1)}$	(0,0,0)	(1,0,0)	(0,1,0)	(0,0,1)
$\Delta_2^{(1)}$	(0,0,0)	(0,1,0)	(0,0,1)	(1,0,0)
$\Delta_3^{(1)}$	(0,0,0)	(0,0,1)	(1,0,0)	(0,1,0)

We further choose $p = 2$ for all edges, $N = 2$ and get the partition shown in Figure 3.6 for $S^{(1)}$.

In the last step the trial functions on S are defined. We start again the construction on \square , given N, p and a further parameter $i^* \in \mathbf{N}_0$. For simplicity we choose only the two following interpolation formulas for functions $f \in \mathcal{C}(\square)$:

$$(3.14) \quad \left. \begin{aligned} (P_0 f)(\phi, r) &:= f(\xi^{(0)}) p^{[0]}(\phi, r) \\ (P_1 f)(\phi, r) &:= \sum_{l=1}^4 f(\xi_l^{(1)}) p_l^{[1]}(\phi, r) \end{aligned} \right\}$$

where

$$(3.15) \quad \left. \begin{aligned} \xi^{(0)} &= (1/2, 1/2) \\ \xi_1^{(1)} &= (c_0, c_0), \quad \xi_2^{(1)} = (c_1, c_0), \\ \xi_3^{(1)} &= (c_0, c_1), \quad \xi_4^{(1)} = (c_1, c_1), \end{aligned} \right\}$$

with the two Gauss points $c_0 \approx 0.211324865405187$ and $c \approx 0.788675134594813$ on $[0, 1]$. The function $p^{[0]}$ is the constant function equal to 1 and the functions $p_l^{[1]}$, $l = 1(1)4$, are the bilinear functions

$$(3.16) \quad \left. \begin{aligned} p_1^{[1]}(\phi, r) &= \frac{(c_1 - \phi)(c_1 - r)}{(c_1 - c_0)^2} \\ p_2^{[1]}(\phi, r) &= \frac{(\phi - c_0)(c_1 - r)}{(c_1 - c_0)^2} \\ p_3^{[1]}(\phi, r) &= \frac{(c_1 - \phi)(r - c_0)}{(c_1 - c_0)^2} \\ p_4^{[1]}(\phi, r) &= \frac{(\phi - c_0)(r - c_0)}{(c_1 - c_0)^2} \end{aligned} \right\}$$

For $i^* \in \mathbf{N}_0$ the set of indices $\{1, \dots, \nu_{N,p}\}$ are divided into two subsets

$$(3.17) \quad \left. \begin{aligned} I_{N,p,i^*} &:= \left\{ \begin{aligned} &\{j \in \{1, \dots, \nu_{N,p}\} \mid \square_j^{N,p} \in \mathbf{L}_{N,p,i^*}, \\ &i < (i^*)^{1/(1+p)} N^{1/(1+1/p)} \}, \quad i^* \geq 1, \\ &\emptyset \end{aligned} \right\} \\ \bar{I}_{N,p,i^*} &:= \{1, \dots, \nu_{N,p}\} \setminus I_{N,p,i^*}. \end{aligned} \right\} \begin{aligned} & \\ & \text{otherwise,} \end{aligned}$$

where (ϕ_j, r_j) is the lower left corner of $\square_j^{N,p}$ and we define $a/0 := +\infty$, if $a > 0$. We use the constant interpolation projector P_0 on $\square_j^{N,p}$, $j \in I_{N,p,i^*}$, and the linear interpolation projector P_1 on $\square_j^{N,p}$, $j \in \bar{I}_{N,p,i^*}$. This defines the interpolation projector P_{n,p,i^*} in $\mathcal{C}(\square)$:

$$(3.18) \quad \left. \begin{aligned} (P_{N,p,i^*} f)(\phi, r) &:= \sum_{j \in I_{N,p,i^*}} f(\tau^{-1}(\xi^{(0)})) p_{N,p,j}^{\square,0}(\phi, r) \\ &+ \sum_{j \in \bar{I}_{N,p,i^*}} \sum_{l=1}^4 f(\tau^{-1}(\xi_l^{(1)})) p_{N,p,j,l}^{\square,1}(\phi, r) \end{aligned} \right\}$$

where the functions $p^{\square,0}$ and $p^{\square,1}$ are local copies of $p^{[0]}$ and $p^{[1]}$:

$$(3.19) \quad \left. \begin{aligned} p_{N,p,j}^{\square,0}(r, \phi) &:= \mathbf{1}_{\square_j^{N,p}}(\phi, r) \\ p_{N,p,j,l}^{\square,1}(r, \phi) &:= \mathbf{1}_{\square_j^{N,p}}(\phi, r) p_l^{[1]}(\tau_{N,p,j}(r, \phi)). \end{aligned} \right\}$$

The parameter i^* controls the neighborhood of $\phi = 0$, respectively $r = 0$, where we use constant interpolation. $i^* = 0$ implies that we use only linear interpolation and a growing i^* increases the number of elements where the constant interpolation is applied. The reason to introduce i^* is the fact that even in two dimensions there is no proof for the stability of the collocation method for the radiosity equation without such a modification. The number $\tilde{\nu}_{N,p,i^*}$ of trial functions introduced on \square is given by

$$(3.20) \quad \tilde{\nu}_{N,p,i^*} = |I_{N,p,i^*}| + 4|\bar{I}_{N,p,i^*}|$$

$$(3.21) \quad = O_{N \rightarrow \infty}(\nu_{N,p}).$$

If we assume that we have for all triangles Δ_j of S three grading exponents $p_l^{(j)}$, $l = 1, 2, 3$, along the edges and, if we choose N and i^* independent of j , we get

$$(3.22) \quad \nu_{N,i^*}(S) := \sum_{j=1}^N 2 \sum_{l=1}^3 \tilde{\nu}_{N,p_l^{(j)},i^*}$$

trial functions on S and the same number of interpolation respectively collocation points. The trial functions, respectively the collocation points on S , are defined by

$$(3.23) \quad p_{S,N,i^*,j} \quad \text{respectively} \quad \xi_{S,N,i^*,j}, \quad j = 1(1)\nu_{N,i^*}(S).$$

We have not indicated the dependence on all grading exponents in the above notation and if possible we will also neglect the indices S and i^* . The typical function $p_{N,k}$ defined on S_j is given by

$$(3.24) \quad p_{N,k}(x) := p_{N,p_i^{(j)},l,m}^{\square,0/1}(\chi(\kappa_h(\Psi_j(x)))),$$

where $j \in \{1, \dots, n\}$, $h \in \{1, \dots, 6\}$, $i \in \{1, 2, 3\}$ and m is only necessary in the case of linear trial functions. A typical interpolation point $\xi_{N,k} \in S_j$ is given by

$$(3.25) \quad \xi_{N,k} = \Psi_j^{-1}(\kappa_h^{-1}(\chi^{-1}(\tau_{N,p_i^{(j)},l}(\xi_m^{(0)/(1)}))))),$$

$h \in \{1, \dots, 6\}$, $i \in \{1, 2, 3\}$, $l \in \{1, \dots, \tilde{\nu}_{N,p,i^*}\}$ and m is only necessary in a rectangle with linear trial functions. The interpolation operator \mathcal{P}_{N,i^*} for a function $f \in \mathcal{C}_R(S)$ is given by

$$(3.26) \quad (\mathcal{P}_{N,i^*}f)(x) := \sum_{j=1}^{\nu_{N,i^*}(S)} f(\xi_{N,i^*,j})p_{N,i^*,j}(x).$$

The linear space of trial functions, given all of the above parameters, will be denoted by

$$(3.27) \quad \Pi_{N,i^*}(S).$$

Because of the transformation χ the functions $p_{N,i^*,j}$ are nonlinear functions and their support has a curved boundary. The advantage of the transformation χ is that we use polar coordinates for the interpolation of the function $f \in \mathcal{C}_R(S)$. So we get

$$(3.28) \quad \lim_{N \rightarrow \infty} \|f - \mathcal{P}_{N,i^*}f\|_{L^\infty(S)} = 0.$$

We again look at our example $S^{(1)}$, with $N = 2$, $p = 2$ and $i^* = 0$ for every edge (Figure 3.7). The second picture shows $S^{(1)}$ with $N = 2$, $p = 2$ and $i^* = 1$ for every sub triangle (Figure 3.8).

After the introduction of this notation it is now easy to formulate the collocation method for the approximate solution of (1.1). Given

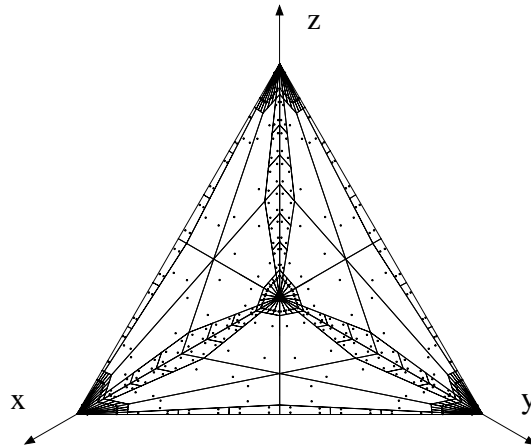


FIGURE 3.7. The collocation points for $S^{(1)}$, with $i^* = 0$ and $\varphi_{2,2}$ is used for all sub triangles.

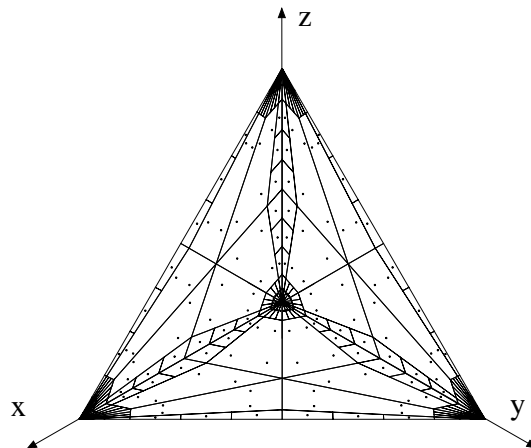


FIGURE 3.8. The collocation points for $S^{(1)}$, with i^* chosen such that one row is used for constant interpolation, and $\varphi_{s,2}$ is used for all sub triangles.

$N \in \mathbf{N}$, $i^* \in \mathbf{N}_0$, $p_i^{(j)} \in [1, \infty)$, $j = 1(1)n$, $i = 1, 2, 3$, the approximate solution $\bar{u}_{N,i^*} \in \Pi_{N,i^*}$

$$(3.29) \quad \bar{u}_{N,i^*} = \sum_{k=1}^{\nu_{N,i^*}(S)} \bar{a}_k p_{N,i^*,k}, \quad \bar{a}_k \in \mathbf{R},$$

is given by the solution of the linear equations system of

$$(3.30) \quad \bar{a}_j - \sum_{k=1}^{\nu_{N,i^*}(S)} \bar{a}_k (\mathcal{K}_{SP_{N,i^*,k}})(\xi_{N,i^*,j}) = E(\xi_{N,i^*,j}), \quad j = 1(1)\nu_{N,i^*}(S).$$

The question of the solvability of (3.30) and the convergence of $\bar{u}_{N,i^*} \rightarrow \bar{u}$, $\bar{u} \in \mathcal{C}_R(S)$ the solution of (1.1), will be addressed in the following remark.

Remark 3.1. a. In 3.14 it is possible to choose any fixed interpolation formula instead of P_1 . See [2] or [21] for interpolation formulas with higher degree.

b. The curved boundary of the support of our trial functions $P_{N,i^*,j}$ does not introduce a problem for the computation of the matrix entries in (3.30), because all numerical integrations are done on the reference square \square . We also need only the mappings χ^{-1} and $D\chi^{-1}$ for the computations, and these mappings are \mathcal{C}^∞ smooth. One disadvantage is the fact that $D\chi^{-1}$ depends on the variables (ϕ, r) on \square . In the numerical computations we cannot put any term involving $D\chi^{-1}$ in front of the integral sign. This would be possible if we would use only linear transformations.

c. The interpolation projectors \mathcal{P}_{N,i^*} and P_{N,p,i^*} are in principle only defined for continuous functions, but we will always consider their extension to $L^\infty(S)$, described in [5].

d. The stability of the above constructed collocation method follows from the results in [12]. Here it was proved that the collocation method is stable. So if i^* and N are sufficiently large the linear system (3.30) is uniquely solvable and the norm of the inverse of the corresponding matrices is bounded if N goes to infinity. In the article [12] the mesh was slightly different, but this has no influence on the i^* modification and the stability.

In the next remark we discuss one of the problems which was encountered during the implementation of the collocation method.

Remark 3.2. Here we give a short description of the algorithm which is used to calculate the entries of the collocation matrix. If we neglect for a moment the nonlinear transformation χ , see (3.5), we see that we must calculate integrals of the form

$$(3.31) \quad \int_0^1 \int_0^1 \frac{c\varepsilon}{((\phi - \phi_0)^2 + (r - r_0)^2 + \varepsilon^2)^2} p_l^{[0]/[1]}(\phi, r) d\phi dr.$$

Here we have transformed one of the elements $\square_k^{N,p}$ on the reference square \square . The constant c is not necessarily small and depends on the normals of the triangle where the collocation point is located and the normal of the triangle $\tilde{\Delta}$, which corresponds to $\square_k^{N,p}$. (ϕ, r, ε) are determined by the relative position of the collocation point to the element $\tilde{\square}_k^{N,p}$ in \mathbf{R}^3 , which corresponds to $\square_k^{N,p}$. The trial functions $p_l^{[0]/[1]}$ are always polynomials and are of degree zero or one in our context. The value ε is determined by the orthogonal distance of the collocation point to the plane E which contains $\tilde{\square}_k^{N,p}$. The values ϕ_0 and r_0 are the coordinates of the projection of the collocation point onto the plane E relative to $\tilde{\square}_k^{N,p}$.

If we use $N = 8$ and $p = 2$ for our example domain $S^{(1)}$, see (3.13), the smallest values of ε are about 10^{-6} . So the function under the integral sign in (3.31) has a maximal value of about 10^{18} and the smallest values are about 10^{-6} . It is clear that the above integral is not easy to compute. In an example we found that a trapezoidal rule with about 4 million points calculated only the first digit of the integral exactly and a Gaussian quadrature with 30 points had no exact digit. This is easy to understand if one tries to plot the graph of the above function.

As a model for the above integral we use the modified Runge function

$$(3.32) \quad I_{\varepsilon,a} := \int_0^1 \frac{\varepsilon}{((x-a)^2 + \varepsilon^2)^2} dx, \quad \varepsilon > 0.$$

Then we use the transformation $x = t_{a,\varepsilon}(y)$, $t_{a,\varepsilon} : [0, 1] \rightarrow [0, 1]$, defined by

$$(3.33) \quad t_{a,\varepsilon}(y) := \begin{cases} y^q & a < 0, \\ (\alpha_1 y - \alpha_2)^q + a & a \in [0, 1], \\ 1 - y^q & a > 1, \end{cases}$$

$$(3.34) \quad q = q(a, \varepsilon) := \begin{cases} \text{odd} \left(\frac{\ln(\sqrt{\varepsilon^2 + a^2})}{\ln(0.3)} \right) & a < 0, \\ \text{odd} \left(\frac{\ln(|e|)}{\ln(0.3)} \right) & a \in [0, 1], \\ \text{odd} \left(\frac{\ln(\sqrt{\varepsilon^2 + (1-a)^2})}{\ln(0.3)} \right) & a > 1, \end{cases}$$

and

$$(3.35) \quad \left. \begin{aligned} \alpha_1 &:= (1-a)^{1/q} + a^{1/q}, \\ \alpha_2 &:= a^{1/q}. \end{aligned} \right\}$$

Here the function $\text{odd}(z)$ determines the smallest odd natural number larger or equal to z . The transformation was motivated by the even simpler integral

$$\int_{-1}^1 \frac{1}{(x^2 + \varepsilon^2)^2} dx, \quad \varepsilon > 0.$$

If we choose the transformation $x = y^q$, q an odd natural number, the poles at $\pm i\varepsilon$ of the function $1/(x^2 + \varepsilon^2)$ are transformed into the $2q$ poles of the function $1/(y^{2q} + \varepsilon^2)$. The distance of these poles from the origin is given by $\varepsilon^{1/q}$. So if we choose

$$q \approx \frac{\ln(\varepsilon)}{\ln(0.3)}$$

then the absolute value is always approximately 0.3, independent of ε . But we remark that the angle of the unit root in the complex domain is neglected here. This transformation will be the subject of a further study. The value 0.3 is chosen because in some experiments 0.3 worked a little bit better than 0.2 or 0.4. Now we denote by $T_{\varepsilon,a,K}$ the value of the trapezoidal rule with 2^K points applied directly to the integral (3.32) and by $\tilde{T}_{\varepsilon,a,K}$ the value of the trapezoidal rule applied to the integral after the variable substitution (3.33) has been applied. Then we look for the smallest natural number K_0 such that

$$(3.36) \quad K_0 := \min\{K \in \mathbf{N} \mid |I_{\varepsilon,a} - T_{\varepsilon,a,K}| < 10^{-8}|I_{\varepsilon,a}|\}$$

respectively

$$(3.37) \quad \tilde{K}_0 := \min\{K \in \mathbf{N} \mid |I_{\varepsilon,a} - \tilde{T}_{\varepsilon,a,K}| < 10^{-8}|I_{\varepsilon,a}|\}.$$

The definition implies that 2^{K_0} , respectively $2^{\tilde{K}_0}$, denote the number of points which are necessary in the trapezoidal rule to get an accuracy of eight digits. The following table shows the effect of the transformation.

TABLE 3.1. The K_0 and \tilde{K}_0 values, see (3.36) and (3.37), for different values of ε and a .

$\varepsilon = 10^{-2}$			$\varepsilon = 10^{-4}$			$\varepsilon = 10^{-6}$		
a	\tilde{K}_0	K_0	a	\tilde{K}_0	K_0	a	\tilde{K}_0	K_0
-0.5	14	17	-0.5	14	17	-0.5	14	17
-0.4	14	17	-0.4	14	17	-0.4	14	17
-0.3	13	17	-0.3	13	17	-0.3	13	17
-0.2	13	18	-0.2	13	18	-0.2	13	18
-0.1	12	19	-0.1	12	19	-0.1	12	19
0.0	7	11	0.0	10	18	0.0	12	>20
0.1	13	13	0.1	9	18	0.1	10	>20
0.2	11	11	0.2	9	18	0.2	10	>20
0.3	10	11	0.3	9	18	0.3	10	>20
0.4	10	11	0.4	9	18	0.4	10	>20
0.5	10	11	0.5	9	18	0.5	10	>20
0.6	10	11	0.6	9	18	0.6	10	>20
0.7	10	11	0.7	9	18	0.8	10	>20
0.8	11	11	0.8	9	18	0.8	10	>20
0.9	13	13	0.9	9	18	0.9	10	>20
1.0	7	11	1.0	10	18	1.0	12	>20
1.1	12	19	1.1	12	19	1.1	12	19
1.2	13	18	1.2	13	18	1.2	13	18
1.3	13	17	1.3	13	17	1.3	13	17
1.4	14	17	1.4	14	17	1.4	14	17
1.5	14	17	1.5	14	17	1.5	14	17

The result is that at least in the range of ε values, which we encounter in the numerical computations, the transformation can reduce the number of necessary quadrature points by a factor of 1000 in one dimension and

so by about 10^6 in two dimension. In the actual computations we use Gaussian formulas, where experiments show that about 130 points (in each dimension if $\varepsilon = 10^{-6}$) are necessary to get an accuracy of six digits.

In practice we determine for every square, where we calculate the entry of the collocation matrix, an approximation for r_0 and ϕ_0 and then use the above transformation in both directions. Remember here also that the real integration area has a curved boundary in the R^3 domain, so an exact value of r_0 and ϕ_0 is difficult to get. But even then the above transformation results in an enormous speed up of the convergence for the trapezoidal rule and the Gaussian rules. Without this transformation a calculation of the above integrals with $\varepsilon = 10^{-6}$ seems to be totally impossible.

But we would like to mention that the number of integrals is small, where such extreme functions have to be integrated, but their influence on the computation time of the collocation matrix is not negligible.

4. Numerical examples. In this section we present the results of several numerical calculations which show the applicability of the collocation method, presented in Section 3. The aim of this section is to verify the theoretical results, which were given in Section 2 and in the articles [17, 10, 11]. So we use only very simple surfaces S with no occlusion and try to calculate the solution with a high precision in order to estimate the order of convergence. We do not want to prescribe the solution because it is one of our goals to work without any assumption on the asymptotics of our solution. But we choose only very simple righthand sides because our previous analysis shows that this should be sufficient to produce nonsmooth solutions. Because of this we do not have a reference solution and we will always take the calculated solution with the highest number of degrees of freedom as the reference solution.

In all our examples the emissivity function and the reflectivity function ρ is constant on each of the triangles Δ_i of the surface S . Furthermore the modification parameter i^* , see (3.17), is always set to zero because, in our numerical experiments, we never detected any problems with the stability of our method. The construction in Section 3 allows us to choose different values for N and the grading exponent p

on every one of the six sub triangles $\Delta_{*,l}$, $l = 1(1)6$, for every triangle Δ_j of S . But we will always take the same N and p for all sub triangles. Together with the piecewise linear trial functions introduced in (3.15)–(3.16), the collocation method is therefore well defined if N and p are given.

For the first example we use the surface $S^{(1)}$ from Section 3 and the emissivity and reflectivity are given according to the following table.

TABLE 4.1. The surface $S^{(1)}$ with the reflectivity function ρ and the emissivity E .

$S^{(1)}$						
triangle	vertices			normal	ρ	E
$\Delta_1^{(1)}$	$(0, 0, 0)^T$	$(1, 0, 0)^T$	$(0, 1, 0)^T$	$(0, 0, 1)^T$	0.5	0.5
$\Delta_2^{(1)}$	$(0, 0, 0)^T$	$(0, 1, 0)^T$	$(0, 0, 1)^T$	$(1, 0, 0)^T$	0.5	1.0
$\Delta_3^{(1)}$	$(0, 0, 0)^T$	$(0, 0, 1)^T$	$(1, 0, 0)^T$	$(0, 1, 0)^T$	0.5	0.3

To get an impression of the solution Figure 4.1 shows the radiosity viewed from $(5, 5, 5)^T$ with a viewing direction towards the origin.

The solution looks smooth and even for our coarsest triangulation the results are so accurate (see the following table) that this is enough for a graphical representation. But the behavior of the solution near the edges is not smooth as the following discussion shows.

First we will use no grading, so $p = 1$, see (3.6)–(3.8). We calculate approximations $\bar{u}_{N,0}$, for $N = 2^i$, $i = 0(1)5$. To estimate the error in the $L^\infty(S^{(1)})$ norm we calculate the approximate solutions at 10000 points within every sub triangle $\Delta_{*,l}$, $l = 1(1)6$, and this for every triangle $\Delta_j^{(1)}$, $j = 1, 2, 3$. So we approximate $\|\cdot\|_{L^\infty(S^{(1)})}$ by a maximum over 180000 points $\omega_i \in S^{(1)}$ on $S^{(1)}$. We denote this semi-norm by

$$(4.1) \quad \|u\|_{L^\infty(S^{(1)}), \text{disc}} := \max_{\omega_i} \{|u(\omega_i)|\}.$$

The following table shows the results.

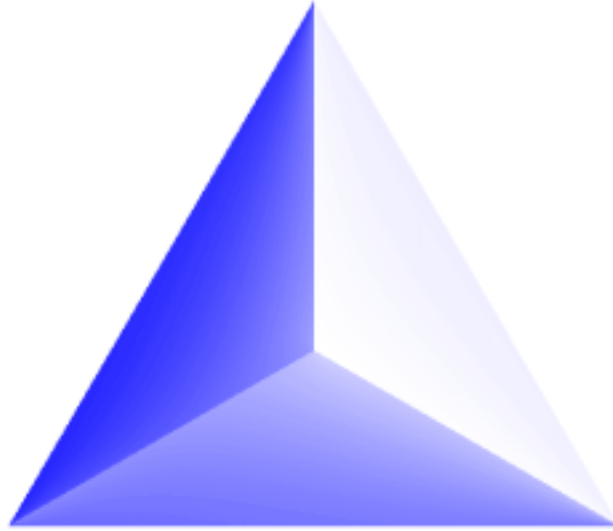
FIGURE 4.1. The radiosity distribution on $S^{(1)}$.

TABLE 4.2. The convergence results for the first example with no grading.

Surface $S^{(1)}$, $i^* = 0$, $p = 1$.				
N	degrees of freedom	$\ \bar{u}_{N,0} - \bar{u}_{32,0}\ _{L^\infty(S^{(1)}), \text{disc}}$	relative improvement	EOC
1	72	2.83248×10^{-2}		
2	288	1.37551×10^{-2}	2.06	0.99
4	1152	6.80114×10^{-3}	2.02	0.90
8	4608	3.21527×10^{-3}	2.11	0.81
16	18432	1.20771×10^{-3}	2.66	0.73
32	73728			

The estimated order of convergence is calculated under the assumption that

$$(4.2) \quad \bar{u}_{N,p}(x_{\max}, y_{\max}) = \bar{u}(x_{\max}, y_{\max}) + \frac{c_1}{N^\alpha}$$

holds. Here (x_{\max}, y_{\max}) is the position where the maximal error occurs and this position should not vary with N . We would like to remark that this is not fulfilled in practice. But, if we assume this, the column EOC in the above table gives the estimated value for α . Especially we take into account that we do not compare our approximate solutions with a known solution, but with a more accurate approximation according to formula (4.2). The numbers in the above table show clearly that the solution \bar{u} is not a smooth function, because all EOC values are smaller than 2. From the analysis in [17, 10, 11], we expect an exponent

$$(4.3) \quad \beta_1 \approx 0.763$$

which describes the ϕ dependence of the solution orthogonal to the edge. This value cannot be found in our table, but it is included in the range of the EOC values, which we calculate. Here we have also neglected the fact that the dependence on the r variable is not clear in the moment. If we assume that u has an asymptotic expansion of the form

$$(4.4) \quad \bar{u}(\phi, r) \approx u(0, \phi) + U_r r^{\beta_2},$$

$$(4.5) \quad \bar{u}(\phi, 0) \approx u(0, 0) + U_\phi \phi^{\beta_1},$$

we can estimate β_1 and β_2 from our numerical results. If we do this for $\bar{u}_{32,1}$ restricted to the surface $\Delta_1^{(1)}$, we get the result

$$(4.6) \quad \beta_1 \approx 0.84, \quad \beta_2 \approx 0.8.$$

Here the values 0.84 and 0.8 depend on the points which we use for the estimate, but we remark that these values vary only in a range of about 0.02 in our experiments. So the numerical results clearly indicate that the solution is not smooth orthogonal to the edge and near the vertices, but an accurate estimate of the kind of singularity seems to be impossible with the above results.

Our main result from Section 2 was that the solution is not necessarily continuous with respect to the Euclidean norm near the vertices. To illustrate this we define the curve

$$(4.7) \quad \alpha_r(t) := r \begin{pmatrix} \cos\left(\frac{\pi}{2}t\right) \\ \sin\left(\frac{\pi}{2}t\right) \\ 0 \end{pmatrix}, \quad t \in [0, 1].$$

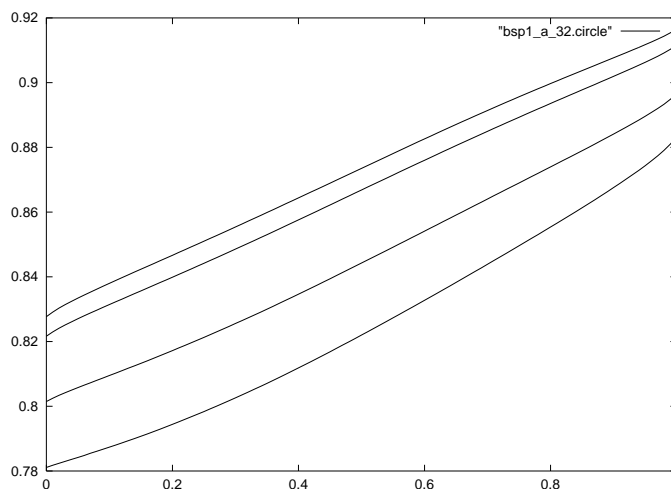


FIGURE 4.2. The function $\bar{u}_{32,0}(\alpha_r(\cdot))$, $r = 0.1$, $r = 0.05$, $r = 0.01$ and $r = 0.001$. With smaller r the functions have larger values. The interval $[0, \pi/2]$ is scaled to $[0, 1]$.

For sufficiently small $r > 0$ the curve α_r lies on $\Delta_1^{(1)}$, and we plot $\bar{u}_{32,0}(\alpha_r(t))$ in the next figure for $r = 0.1$, $r = 0.05$, $r = 0.01$ and $r = 0.001$.

Figure 4.2 indicates that the solution \bar{u} is not continuous near the origin with respect to the usual Euclidean norm; here we remember that Table 4.2 suggests that $\|\bar{u} - \bar{u}_{32,0}\|_{L^\infty(S^{(1)})} \approx 10^{-3}$ holds. So one has to use a triangulation with respect to local polar coordinates to guarantee convergence with respect to the L^∞ norm.

In Figure 4.2 it is nearly impossible to determine the exact behavior of $\bar{u}_{32,0}(\alpha_r(t))$ near $t = 0$ or $t = 1$. Therefore, we calculate with a difference quotient an approximation for

$$\frac{d}{dt} \bar{u}_{N,0}(\alpha_{0.01}(t)),$$

$N = 8, 16, 32$ and get the result shown in Figure 4.3.

Now it shows that there is some kind of singularity near the boundary values 0 and 1. We have not tried to estimate the exponent because, even for our most accurate solution, we expect an error of about 10^{-3} ,

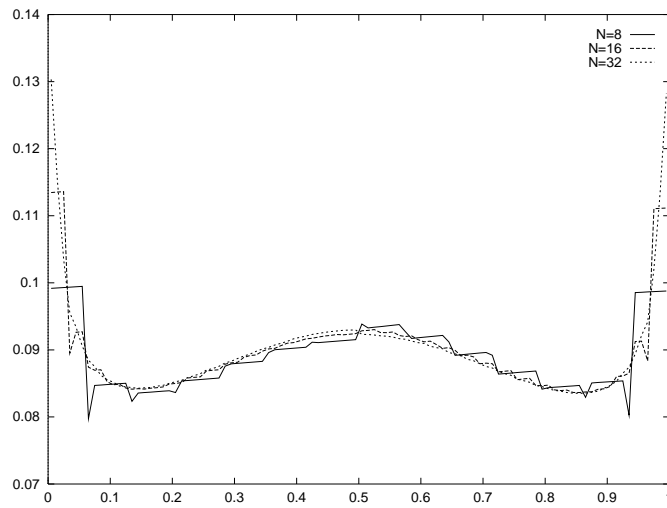


FIGURE 4.3. Three approximations for $\frac{d}{dt}\bar{u}(\alpha_{0.01}(t))$ with $N = 8$, $N = 16$ and $N = 32$, $p = 1$.

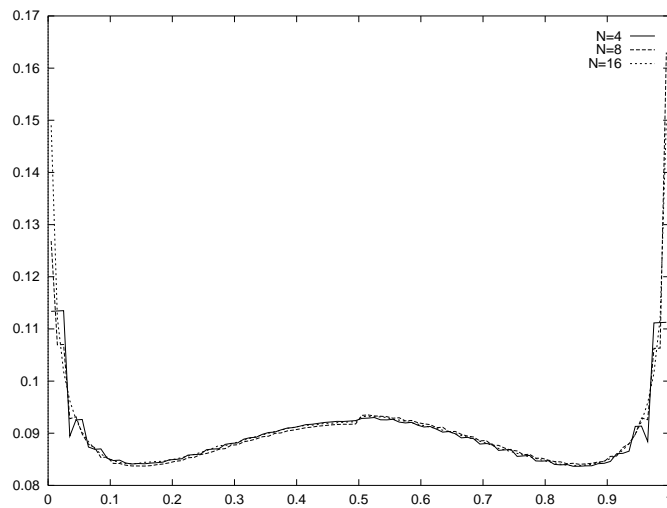


FIGURE 4.4. Three approximations for $\frac{d}{dt}\bar{u}(\alpha_{0.01}(t))$, with $N = 4$, $N = 8$ and $N = 16$, $p = 2$.

see Table 4.2, and the step width for the difference quotient is 10^{-2} . So this also seems not very promising.

In order to increase the order of convergence one can increase the grading exponent. We have chosen $p = 2$ and calculated for different values of N an approximate solution. This grading exponent was used for all triangles and along all edges. We expect that the rate of convergence will be doubled. The estimated convergence rates are shown in Table 4.3.

TABLE 4.3. The convergence result for the first example with exponent $p = 2$.

Surface $S^{(1)}$, $i^* = 0$, $p = 2$.				
N	degrees of freedom	$\ \bar{u}_{N,0} - \bar{u}_{32,0}\ _{L^\infty(S^{(1)})}$, disc	relative improvement	EOC
1	72	2.9553×10^{-2}		
2	576	1.2696×10^{-2}	2.32	1.14
4	3168	4.9290×10^{-3}	2.58	1.18
8	15840	1.2296×10^{-3}	4.01	1.50
16	77760			

The results of the case $p = 1$ are confirmed and this shows that a weakly singular behavior of the solution \bar{u} has to be taken into account if the solution has to be computed with a high accuracy.

Finally we consider another geometrical configuration in order to study the influence on the convergence.

TABLE 4.4. The surface $S^{(2)}$ with the reflectivity function ρ and the emissivity E .

$S^{(2)}$						
triangle	vertices			normal	ρ	E
$\Delta_1^{(2)}$	$(0, 0, 0)^T$	$(1, 0, 0)^T$	$(0, 1, 0)^T$	$(0, 0, 1)^T$	0.5	1.0
$\Delta_2^{(2)}$	$(0, 0, 0)^T$	$(0, 1, 0)^T$	$(1, 1, 1)^T$	$1/\sqrt{2}(1, 0, -1)^T$	1.0	0.2
$\Delta_3^{(2)}$	$(0, 0, 0)^T$	$(1, 1, 1)^T$	$(1, 0, 0)^T$	$1/\sqrt{2}(0, 1, -1)^T$	0.25	0.2

Here the theory of [17, 10, 11] gives us the following Hölder exponents of the solution along the different edges.

TABLE 4.5. The Hölder exponents along the different edges of $S^{(2)}$.

edge between	exponent
$\Delta_1^{(2)}$ and $\Delta_2^{(2)}$	≈ 0.6527
$\Delta_1^{(2)}$ and $\Delta_3^{(2)}$	≈ 0.8782
$\Delta_2^{(2)}$ and $\Delta_3^{(2)}$	≈ 0.7644

Again the numerical results do not exactly show the predicted orders of convergence, but the results indicate a rate which is smaller than in example one.

TABLE 4.6. The convergence results for the second example with no grading.

Surface $S^{(2)}$, $i^* = 0$, $p = 1$.				
N	degrees of freedom	$\ \bar{u}_{N,0} - \bar{u}_{32}\ _{L^\infty(S^{(1)})}$, disc	relative improvement	EOC
1	72	9.69035×10^{-2}		
2	288	5.19997×10^{-2}	1.8635	0.829
4	1152	3.03553×10^{-2}	1.7130	0.588
8	4608	1.56782×10^{-2}	1.9361	0.626
16	18432	6.13000×10^{-3}	2.5576	0.639
32	73728			

The maximal error in the first row, $N = 1$, is found in the middle of the triangle $\Delta_1^{(2)}$, but all other maximal errors are found in $(0, 0.5, 0)^T$. This corresponds to the smallest Hölder exponent along this edge, see Table 4.5. We finish with Figure 4.5, which shows us the solution in the second example.

ENDNOTES

1. The author would like to thank Dr. A. Rathsfeld for this hint.

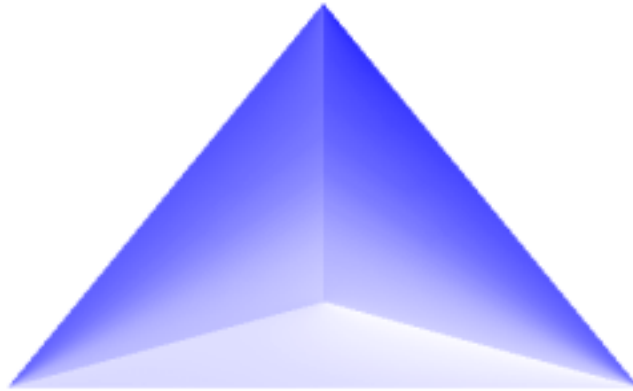


FIGURE 4.5. The radiosity distribution on $S^{(2)}$, viewed from $(5, 5, 2)^T$.

REFERENCES

1. J. Arvo, K. Torrance and B. Smits, *A framework for the analysis of error in global illumination algorithms*, Computer Graphics (ACM SIGGRAPH '94 Proceedings), 1994, pp. 75–84.
2. K. Atkinson, *The numerical solution of integral equations of the second kind*, Cambridge University Press, Cambridge, 1997.
3. ———, *The planar radiosity equation and its numerical solution*, IMA J. Numer. Anal. **20** (2000), 303–332.
4. K. Atkinson and G. Chandler, *The collocation method for solving the radiosity equation for unoccluded surfaces*, J. Integral Equations Appl. **10** (1998), 253–289.
5. K. Atkinson, I. Graham and I. Sloan, *Piecewise continuous collocation for integral equations*, SIAM J. Numer. Anal. **20** (1983), 172–186.
6. K. Atkinson, D.D-K. Chien and J. Seol, *Numerical analysis of the radiosity equation using the collocation method*, Elec. Trans. Numer. Anal. **11** (2000), 94–120.
7. F.C. Cohen and J.R. Wallace, *Radiosity and realistic image synthesis*, Academic Press, Cambridge, MA, 1993.
8. J. Elschner, *On spline approximations for a class of non-compact integral equations*, Math. Nachr. **146** (1988), 271–321.
9. A. Erdélyi, W. Magnus, F. Oberhettinger and F.G. Tricomi, *Tables of integral transforms*, Vol. 1, McGraw-Hill Book Co., Inc., New York, 1954.

10. O. Hansen, *The local behavior of the solution of the radiosity equation on polyhedral domains in \mathbf{R}^3* , SIAM J. Math. Anal. **33** (2001), 718–750.
11. ———, *The mapping properties of the radiosity operator along an edge*, J. Math. Methods Appl. Sci. **25** (2002), 1075–1090.
12. ———, *On the stability of the collocation method for the radiosity equation on polyhedral domains*, IMA J. Numer. Anal. **22** (2002), 463–479.
13. J.T. Kajiya, *The rendering equation*, Computer Graphics (ACM SIGGRAPH '84 Proceedings), 1986, pp. 143–150.
14. J. Král, *Integral operators in potential theory*, Lecture Notes in Math., vol. 823, Springer-Verlag, Berlin - New York, 1980.
15. P. Moon and D.E. Spencer, *The photic field*, MIT Press, Massachusetts, 1981.
16. N. Qatanani, *Lösungsverfahren und Analysis der Integralgleichung für das Hohlraum-Strahlungs-Problem*, Ph.D. Thesis, Universität Stuttgart, 1996 (in German).
17. A. Rathsfield, *Edge asymptotics for the radiosity equation over polyhedral boundaries*, Math. Methods Appl. Sci. **22** (1999), 217–241.
18. C. Schwab and W. Wendland, *On numerical cubatures of singular surface integrals in boundary element methods*, Numer. Math. **62** (1992), 343–369.
19. R. Siegel, J.R. Howell and K. Lohrengel, *Wärmeübertragung durch Strahlung*, Vols. 1 and 2, Springer-Verlag, Berlin, 1988 (in German).
20. F.X. Sillion and C. Puech, *Radiosity & global illumination*, Morgan Kaufmann Publ., San Francisco, 1994.
21. A.H. Stroud, *Approximate calculation of multiple integrals*, Prentice Hall, Inc., Englewood Cliffs, NJ, 1971.
22. T. Tiihonen, *Stefan-Boltzmann radiation on non-convex surfaces*, Math. Methods Appl. Sci. **20** (1997), 47–57.
23. ———, *Finite element approximation of nonlocal heat radiation problems*, Math. Models Methods Appl. Sci. **8** (1998), 1071–1089.
24. T. Tiihonen and M.T. Laitinen, *Integro-differential equation modelling heat transfer in conducting, radiating and semitransparent materials*, Math. Methods Appl. Sci. **21** (1998), 375–392.
25. A. Watt and M. Watt, *Advanced animation and rendering techniques*, Addison Wesley, ACM Press, New York, 1992.

FACHBEREICH MATHEMATIK, JOHANNES-GUTENBERG UNIVERSITÄT MAINZ, SAAR-
STR. 21, 55099 MAINZ, GERMANY
E-mail address: hansen@mathematik.uni-mainz.de